NAVAL POSTGRADUATE SCHOOL

MONTEREY, CALIFORNIA

THESIS

NUMERICAL SIMULATIONS, MEAN FIELD THEORY AND MODULATIONAL STABLITY ANALYSIS OF THERMOHALINE INTRUSIONS

by

Mark A. Hebert

September 2011

Thesis Advisor: Timour Radko
Second Reader: Jason Flanagan

Approved for public release; distribution is unlimited

THIS PAGE INTENTIONALLY LEFT BLANK

REPORT DOCUMENTATION PAGE			*Form Approved OMB No. 0704-0188*
Public reporting burden for this collection of information is estimated to average 1 hour per response, including the time for reviewing instruction, searching existing data sources, gathering and maintaining the data needed, and completing and reviewing the collection of information. Send comments regarding this burden estimate or any other aspect of this collection of information, including suggestions for reducing this burden, to Washington headquarters Services, Directorate for Information Operations and Reports, 1215 Jefferson Davis Highway, Suite 1204, Arlington, VA 22202-4302, and to the Office of Management and Budget, Paperwork Reduction Project (0704-0188) Washington DC 20503.			
1. AGENCY USE ONLY ***(Leave blank)***	**2. REPORT DATE** September 2011	**3. REPORT TYPE AND DATES COVERED** Master's Thesis	
4. TITLE AND SUBTITLE Numerical Simulations, Mean Field Theory and Modulational Stability Analysis of Thermohaline Intrusions		**5. FUNDING NUMBERS**	
6. AUTHOR(S) Mark A. Hebert			
7. PERFORMING ORGANIZATION NAME(S) AND ADDRESS(ES) Naval Postgraduate School Monterey, CA 93943-5000		**8. PERFORMING ORGANIZATION REPORT NUMBER**	
9. SPONSORING /MONITORING AGENCY NAME(S) AND ADDRESS(ES) N/A		**10. SPONSORING/MONITORING AGENCY REPORT NUMBER**	
11. SUPPLEMENTARY NOTES The views expressed in this thesis are those of the author and do not reflect the official policy or position of the Department of Defense or the U.S. Government. IRB Protocol Number ____N/A_____			
12a. DISTRIBUTION / AVAILABILITY STATEMENT Approved for public release; distribution is unlimited		**12b. DISTRIBUTION CODE** A	

13. ABSTRACT (maximum 200 words)

Thermohaline intrusions are produced by lateral shear advection across thermal and haline fronts, self-driven via double-diffusion, and cause significant lateral fluxes. The primary goal of this thesis is to understand the mechanisms responsible for their development and equilibration. Previous theories (mean-field models) were limited by their reliance on the vertical flux laws, which still remain a great source of uncertainty and require modelers to assume that intrusion development is uniquely determined by the background gradients. An alternative approach, based on the multiscale mechanics, views intrusions as modulational instability of the rapidly varying salt fingers. We present an exhaustive study on the effects of background parameters on the vertical and horizontal fluxes of temperature and salinity using two-dimensional numerical simulations. Specific experiments are designed to identify the most promising theoretical techniques for predicting intrusion evolution. Based on numerical results, the assessments of the two theoretical models are made and the mean field theory is found to be superior. Growth rates are calculated as a function of inclination of intrusions, which is used to determine the dominant modes by focusing on the fastest-growing instability. Equilibrium diffusivities are calculated to develop an explicit parameterization for the effects of thermohaline intrusions.

14. SUBJECT TERMS Double-diffusion, double-diffusive convection, diffusive convection, heat flux, salinity flux, Prandtl, Prandtl Number, diffusivity, diffusivity rates, salt fingers, buoyancy, ocean circulation, ocean convection, turbulent mixing			**15. NUMBER OF PAGES** 83
			16. PRICE CODE
17. SECURITY CLASSIFICATION OF REPORT Unclassified	**18. SECURITY CLASSIFICATION OF THIS PAGE** Unclassified	**19. SECURITY CLASSIFICATION OF ABSTRACT** Unclassified	**20. LIMITATION OF ABSTRACT** UU

NSN 7540-01-280-5500 Standard Form 298 (Rev. 2-89)
Prescribed by ANSI Std. 239-18

THIS PAGE INTENTIONALLY LEFT BLANK

Approved for public release; distribution is unlimited

NUMERICAL SIMULATIONS, MEAN FIELD THEORY AND MODULATIONAL STABILITY ANALYSIS OF THERMOHALINE INTRUSIONS

Mark A. Hebert
Lieutenant, United States Navy
B.S., United States Naval Academy, 2005

Submitted in partial fulfillment of the
requirements for the degree of

MASTER OF SCIENCE IN PHYSICAL OCEANOGRAPHY

from the

NAVAL POSTGRADUATE SCHOOL
September 2011

Author: Mark A. Hebert

Approved by: Timour Radko
Thesis Advisor

Jason Flanagan
Second Reader

Jeff Paduan
Chair, Department of Oceanography

THIS PAGE INTENTIONALLY LEFT BLANK

ABSTRACT

Thermohaline intrusions are produced by lateral shear advection across thermal and haline fronts, self-driven via double-diffusion, and cause significant lateral fluxes. The primary goal of this thesis is to understand the mechanisms responsible for their development and equilibration. Previous theories (mean-field models) were limited by their reliance on the vertical flux laws, which still remain a great source of uncertainty and require modelers to assume that intrusion development is uniquely determined by the background gradients. An alternative approach, based on the multiscale mechanics, views intrusions as modulational instability of the rapidly varying salt fingers. We present an exhaustive study on the effects of background parameters on the vertical and horizontal fluxes of temperature and salinity using two-dimensional numerical simulations. Specific experiments are designed to identify the most promising theoretical techniques for predicting intrusion evolution. Based on numerical results, the assessments of the two theoretical models are made and the mean field theory is found to be superior. Growth rates are calculated as a function of inclination of intrusions, which is used to determine the dominant modes by focusing on the fastest-growing instability. Equilibrium diffusivities are calculated to develop an explicit parameterization for the effects of thermohaline intrusions.

THIS PAGE INTENTIONALLY LEFT BLANK

TABLE OF CONTENTS

THIS PAGE INTENTIONALLY LEFT BLANK

LIST OF FIGURES

LIST OF TABLES

THIS PAGE INTENTIONALLY LEFT BLANK

LIST OF ACRONYMS AND ABBREVIATIONS

BonD	Battlespace On Demand
CTD	Conductivity-Temperature-Depth
DNS	Direct Numerical Simulation
ESRL	Earth Systems Research Laboratory
GFDLMOM2	Geophysical Fluid Dynamic Laboratory's Modular Ocean Model 2.
HYCOM	Hybrid Coordinate Ocean Model
K–H	Kelvin–Helmholtz
METOC	Meteorology and Oceanography
FLOPS	Floating Operations Per Second
FY	Fiscal Year
MFTA	Mean Field Theory Analysis
MSA	Modulational Stability Analysis
megaFLOP	10^3 FLOPS
ONR	Office of Naval Research
OGCM	Ocean Global Current Model
petaFLOP	10^{15} FLOPS
ppt	Parts Per Thousand
R&D	Research and Development
T–S	Temperature–Salinity

THIS PAGE INTENTIONALLY LEFT BLANK

ACKNOWLEDGMENTS

I would foremost like to thank my family. Pursuing this level of education in the amount of time allotted to me has been no small feat. Without their love, support and sacrifice, I would not have been able to accomplish this task. I want to especially thank my wife, Christina, for working around my schedule and helping to raise our two wonderful children when I wasn't there physically and mentally. I love you very much.

I would also like to thank Professor Timour Radko for his patience as I stumbled through this very complex subject of double-diffusion and thermohaline intrusions. Your assurance in my ability to tackle such a difficult topic was essential to building my own self-confidence that led to the completion of this thesis. You imparted your expertise onto me in the easiest of ways, breaking down convoluted equations and theories into concepts that were trivial enough to explain to the simplest of minds; namely, my own.

To Jason Flanagan, PhD, I extend my deepest gratitude for your help with FORTRAN and allowing me to expunge all of my frustrations about learning double-diffusion and thermohaline intrusions. Your position as second reader provided valuable inputs to make this topic come out as clearly as possible. I would have been lost in a fog without your help, and completing my thesis ahead of schedule would never have been possible. I am forever in your debt.

Additionally, I cannot go without saying thanks to LT Paul Smith, whose help with working with the computer, guidance in choosing the right thesis advisor and general friendship was invaluable during this whole process. I truly wish you the best of luck in the future and hope to see you again.

Finally, thank you to all my classmates: Frank, Doug, Matt, Chris, Bryan, and Stephanie. Without your help I would have never made it to the point of writing a thesis. Fair winds and following seas to you all.

THIS PAGE INTENTIONALLY LEFT BLANK

I. INTRODUCTION

A. HISTORY

In 1857, W. S. Jevons performed the first laboratory experiments on salt fingers. His experiments, using heat and sugar, produced "long narrow convection cells that formed when warm, sugary water was introduced over cool, fresh water" (Schmitt et al., 2003). While he correctly deduced that this phenomenon was a result of the different diffusivity rates, Jevons, as well as Rayleigh in 1883, failed to identify the key physical mechanism of salt fingering. In doing so, the oceanography community lost nearly a century of study on double-diffusion.

By 1960, Melvin Stern showed that gravitationally stable masses could drive convection if they contained properties with different diffusivities, such as heat and salt. His model used warm, salty over cold, fresh orientation similar to that of Jevons. This theory marked the beginnings for the study of flows that are driven by thermohaline processes, now known as salt fingers. Stern also predicted the possibility of instabilities in the sister case—cold, fresh fluid over a warm, salty fluid, known as "diffusive-convection." Nine years later, thermohaline staircases seen in vertical profiles were shown to be formed via these double-diffusive processes (Stern and Turner, 1969).

Thermohaline staircases in the ocean can span throughout the main thermocline vertically and extend thousands of kilometers horizontally. The realization of their double diffusive origin has moved double-diffusion, a process that occurs on the orders of centimeters, from a trivial pursuit to a potential major driver of diapycnal mixing. Theoretical models, laboratory experiments and, more recently numerical models, are used to quantify double-diffusive fluxes, providing the foundation for research into the importance of this micro-scale feature on the large-scale ocean circulation (Ruddick and Kerr, 2003b).

Another dramatic consequence of double diffusion in the ocean involves thermohaline intrusions, pronounced interleaving, laterally spreading structures commonly observed in the vicinity of fronts and eddies in the oceans. When trying to

quantify the characteristics of intrusions, Stern (1967) initially ignored any corresponding momentum fluxes associated with the vertical transport of temperature and salinity. However, his formulations failed to include a preferred vertical scale. In 1981, Toole and Georgi noted that by taking into account the momentum fluxes it becomes possible to predict the vertical scale of intrusions. Since then, gross estimates of linear theory have been confirmed by laboratory (Ruddick et al., 1999) and direct field measurements (Rudels et al., 1998). However, there still remain many aspects (i.e., dependence of intrusion characteristics on stratification and the relative strengths of the temperature and salinity signatures) that have not been rigorously tested by observations models.

B. MIXING IN THE OCEAN

The circulation of the ocean's water masses acts to homogenize ocean properties throughout its volume. This is achieved through the movement of water in all three spatial directions (North to South, East to West and vertically) accompanied by the continuous exchange of temperature and salinity. This tendency is counteracted by the differential heating, evaporation and precipitation at the sea surface. Understanding the mechanisms involved in the maintenance of the delicate balance between surface forcing and interior mixing is the key problem in physical oceanography. Knowledge of the ocean circulation can be improved by perfecting models and our understanding of the mixing processes. Specifically, there remains much to investigate on the scales of mixing that are currently too small for our global models.

C. GLOBAL ROLE OF THERMOHALINE BALANCE

Understanding the thermohaline balance is critical to understanding the ocean's circulation and mixing processes. Temperature plays a large role in the process and varies widely depending on location, whilst the variation in salinity is about 4 parts per thousand (ppt) only, across the entire ocean. There is no one property that is more important than the other. However, there has been a recent focus on salinity due to its slow variability.

From the perspective of global climate variability, salinity provides insight on the exchange and storage of freshwater. It is an excellent tracer of circulation, which is

important in the redistribution of heat and carbon dioxide. The Climate Variability and Predictability Program (CLIVAR) was created to investigate the "slowly varying components of the climate system" (CLIVAR, 2006). Specifically, the United States is contributing a team of researchers to focus on salinity with the following three objectives:

1) Describe the role of ocean salinity in the global water cycle, global ocean circulation and climate variability.

2) Identifying the requirements and challenges for observing and analyzing salinity, as well as, simulating processes that determining the ocean's role in the transportation and storage of salinity.

3) Provide guidance to the National Aeronautics and Space Administration (NASA) on future activities.

This research directly supports tenets 1 and 2 of CLIVAR's objectives, by helping advance the understanding and modeling of intrusion dynamics, a mechanism driven by the vertical transport of salinity. This thesis is organized as follows. Chapter II discusses the physics of two different types of double-diffusive convection and their relationships with thermohaline intrusions. Additionally, Chapter II describes key features of the direct numerical simulations (DNS) used in our study and introduces the two leading theories explaining the dynamics of thermohaline intrusions. In Chapter III, we present the setup of the numerical model. The results from the models are presented in Chapter IV. Also in Chapter IV, the numerical results are compared to the two governing theories and the large-scale consequences of this newfound understanding is presented as a proposed parameterization algorithm. The results of all models and their intercomparisons are summarized, and the naval impact of this study is presented in Chapter V. Finally, recommendations for future work in this field of study are provided in Chapter VI.

THIS PAGE INTENTIONALLY LEFT BLANK

II. BACKGROUND

A. DOUBLE-DIFFUSIVE CONVECTION

1. Salt Fingering Regime

Double-diffusion occurs in water masses that are stratified, but gravitationally stable. Temperature and salinity have opposite effects on density. This antagonism reveals salt fingering as a fundamental small-scale mixing process in the ocean.

Figure 1 shows the initial conditions necessary for salt fingers to develop, which are warm, salty water above cold, fresh water. This orientation is common in many parts of the world ocean, particularly in the subtropical thermocline where intense solar radiation heats up and evaporates the surface layer, leaving behind a warmer and saltier water mass.

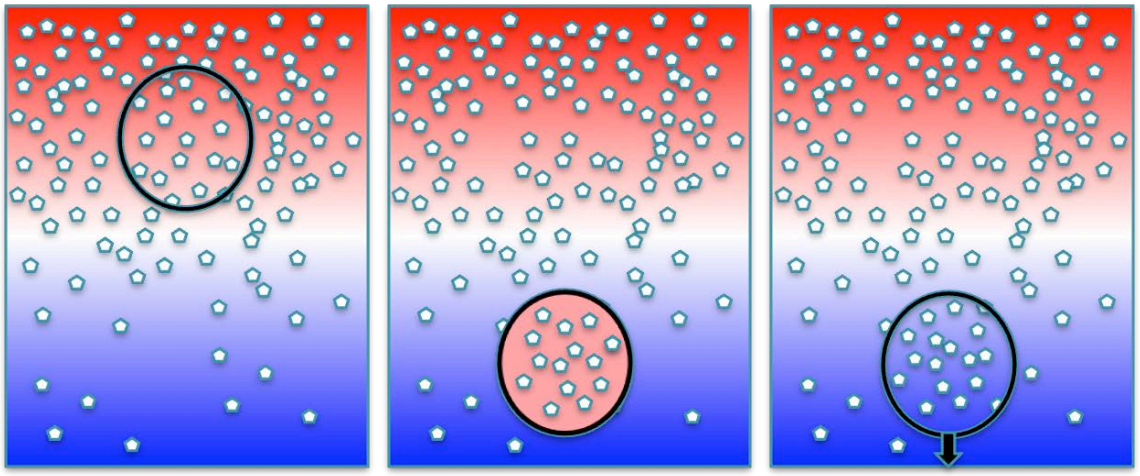

Figure 1. Schematic illustrating dynamics of salt fingers. Warm, salty fluid is located over cold, fresh fluid. Red indicates warm and blue indicates cold fluid. The small pentagons represent salt content. From University of California at Santa Cruz (n.d.)

In fact, salt fingering is a prevalent feature throughout the Atlantic Ocean's thermocline. Figures 2–4, demonstrate the vast extent of salt fingering. You (2002) states that, "in total, about 44% of the oceans display double diffusion, of which 30% is

salt fingering and 14% is diffusive [convection]." Areas of particular concern to the U.S. Navy, namely the Persian Gulf, Mediterranean Sea, and East China Sea, are highly susceptible to double diffusion.

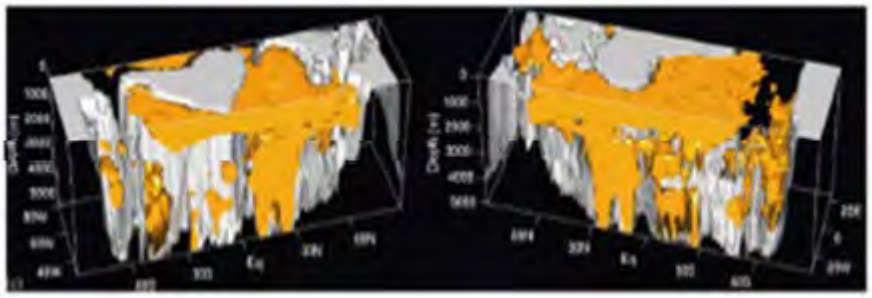

Figure 2. Three-dimensional plot of salt fingering in the western (left-plot) and eastern (right plot) Atlantic Ocean. After You (2002)

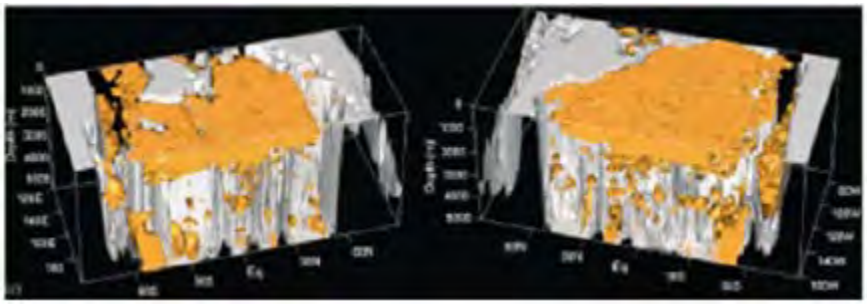

Figure 3. Same as Figure 2, but for the Pacific Ocean

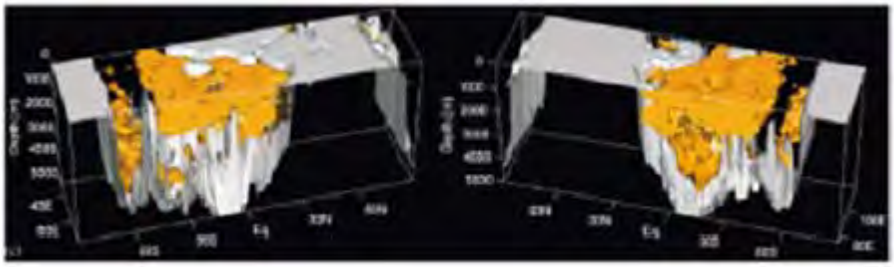

Figure 4. Same as Figure 2, but for the Indian Ocean

With the initial conditions necessary for salt fingering defined, we now explain how heat and salinity affect the density of a parcel of water. Increasing the temperature of a parcel makes the parcel less dense than its surroundings, causing it to rise vertically and stop only when its surroundings are equal to its internal temperature. Therefore, one expects to find warm above cold in a stably-stratified fluid. In contrast, boosting the

salinity of a parcel will increase the density, causing the parcel to be heavier than its surroundings and to sink toward the bottom until it reaches equilibrium. Thus, a saltier layer above a fresh layer would result in an eventual overturning. However, as stated previously, it is the unique combination of heat and salinity, and the competition against one another for control of density-driven dynamics that allows for the development of salt fingering.

It is the differences at the molecular level that hold the key to salt-finger dynamics. Heat diffuses nearly one-hundred times faster than salinity, effectively trapping the salt content within the parcel. As seen in Figures 1 and 5, this parcel initially begins sinking due to its higher density. As it sinks, the parcel is surrounded by cooler, fresher water. Since heat diffuses more rapidly than salinity, the parcel losses heat horizontally to its surroundings, increasing the density and reinforcing the initial downward motion. The surrounding fluid, in turn, becomes warmer and more buoyant, causing it to rise vertically. Thus, there is a net flux of heat and salt vertically across the stratification. Even though most of the heat is diffused horizontally, there is an overall down gradient flux of temperature as well as of salinity. All of the energy required for this mixing arises from the unstable potential energy in the initial salt field (Ruddick and Garrett, 2010).

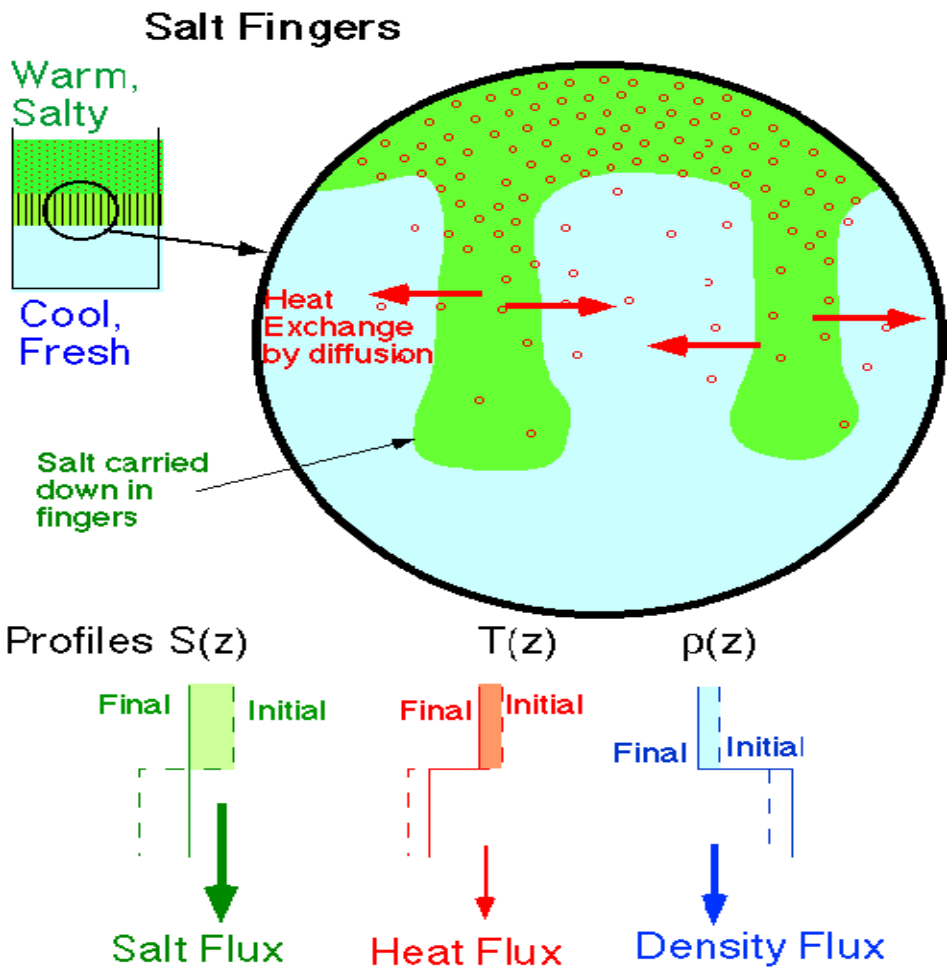

Figure 5. An illustration of salt finger dynamics

Schmidt (1979, 1983) presents the linear solutions for the evolution of salt fingering for all Prandtl numbers, $\Pr = \nu/\kappa_T$, and diffusivity ratios, $\tau = \kappa_S/\kappa_T$, where κ_S is the diffusivity of salinity, κ_T, is the thermal diffusivity and υ is the kinematic viscosity.

For instabilities to occur in the ocean,

$$R_\rho < \frac{\kappa_T}{\kappa_S} \sim 100,$$

where $R_\rho = \alpha T_z / \beta S_z$ is known as the density ratio. This means that the vertical salt gradient required for instabilities can be as low as 1/100th of the temperature gradient

when compared in density units. Additionally, in order to maintain the static stability of the water column necessary for salt fingering, it is required that $R_\rho > 1$. As stated previously, these conditions are commonly met in the world's ocean.

It is also important to distinguish salt fingering from its very different, but equally important, counterpart; diffusive convection will be discussed next in detail to illustrate the differences between the two dynamical phenomena.

2. Diffusive Convection Regime

As mentioned above, double diffusion includes another type of instability operating in the stratification, known as diffusive convection. The dynamic process is recognized by its cold, fresh over warm, salty orientation and is most prevalent in the Arctic regions, as can be seen in Figures 6–8. It is believed that the Arctic is especially susceptible to this process as warm, salty water of Atlantic origin circulates around the perimeter, giving rise to lateral interleaving. In fact, the temperature and salinity signatures of these intrusions have been found to be very coherent over nearly 2000 km, and it has been suggested that this is a very important mechanism in controlling the Arctic climate change (May and Kelley, 2001).

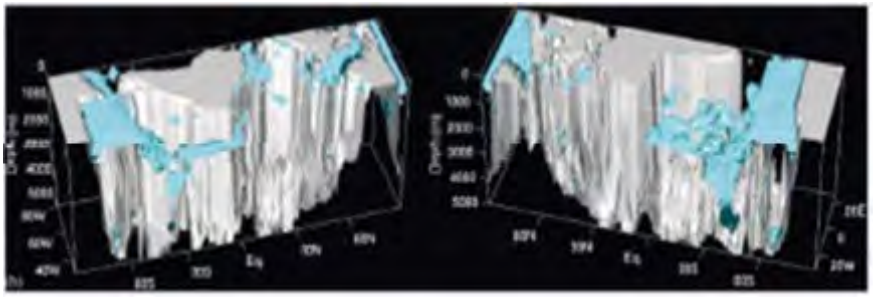

Figure 6. Three-dimensional plot of diffusive convection in the western (left plot) and eastern (right plot) Atlantic Ocean. After You (2002)

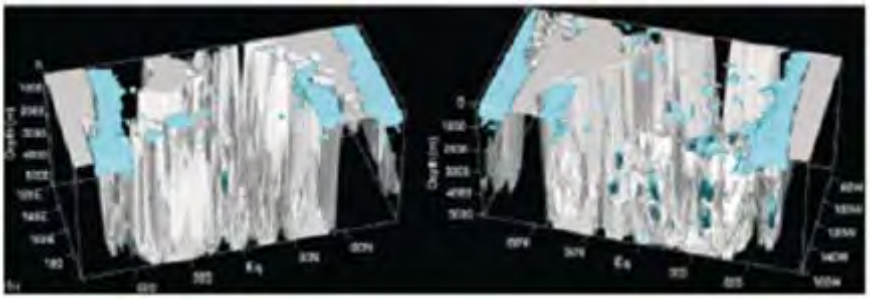

Figure 7. Same as Figure 6, but for Pacific Ocean.

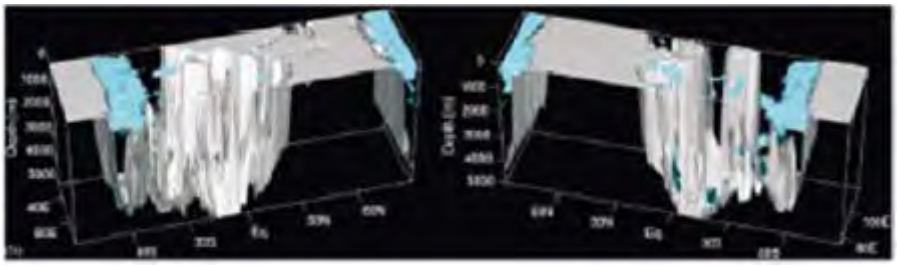

Figure 8. Same as Figure 6, but for Indian Ocean.

The dynamics of oscillatory diffusive convection can be explained by taking a parcel of warm, salty water and displacing it upward. As seen in Figure 9, once the parcel crosses the thin interface into cooler water, the larger thermal diffusivity of temperature forces the parcel to quickly lose its heat to its surroundings. At the same time, the smaller diffusivity of salinity traps the salt content in the parcel and, in combination with cooler temperatures, makes the parcel denser, forcing it to sink back down. This increased density forces the parcel to overshoot its original location. As it overshoots into the warmer layer, it regains its heat and resumes returning upward, leading to an oscillatory pattern known as oscillatory diffusive convection.

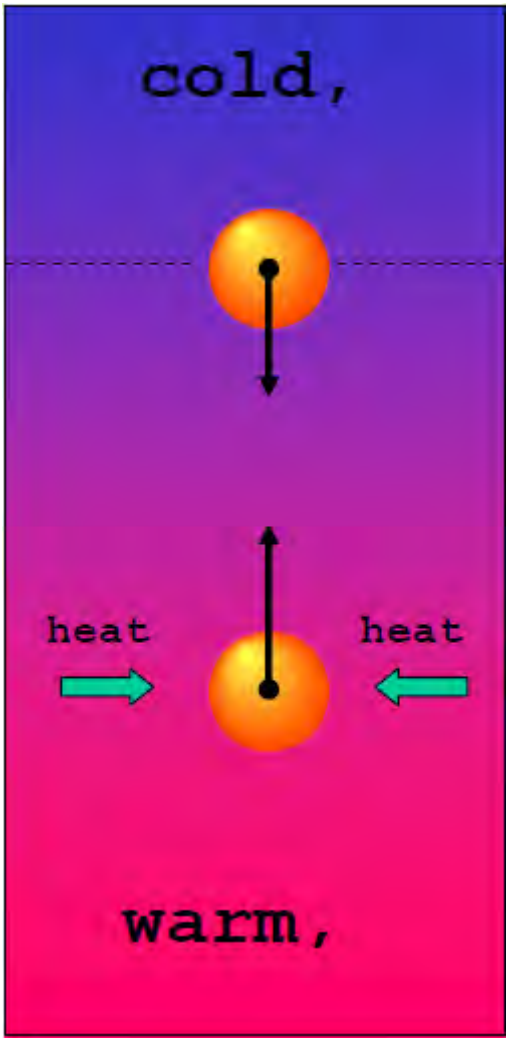

Figure 9. Oscillatory regime of diffusive convection.

Perhaps more commonly researched are patterns of well-mixed layers separated by diffusive interfaces, known as diffusive layering. Figure 10 shows one of these layers in which cold, fresh water lies above warm, salty water. Heat is diffused vertically across the interface, warming particles directly above. At the same time, particles directly below are losing heat as a result of this vertical flux. This warming and cooling causes the rising and falling of particles, respectively, leading to the convection cells above and below the interface. These convection cells maintain a homogenous T–S distribution in each layer.

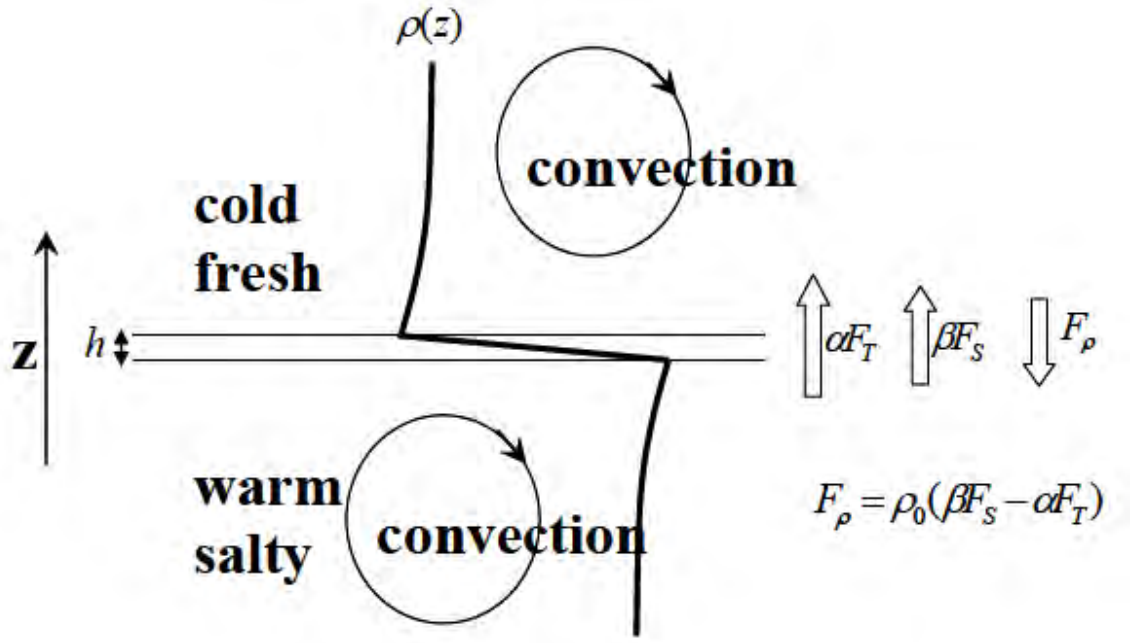

Figure 10. Diffusive layering.

B. THERMOHALINE INTRUSIONS

Intrusions are often identified via conductivity-temperature-depth (CTD) casts via inversions of temperature and salinity with respect to depth. These naturally occurring phenomena are self-driven via double diffusion and the release of potential energy stored in the salt component (Ruddick and Kerr, 2003a). Intrusions are commonly found in areas where there are lateral gradients of temperature and salinity. Common examples are near fronts, currents, eddies and specific geographic regions such as the Arctic, Mediterranean and off the coast of Brazil. Intrusions are produced by lateral shear advection across thermal and haline fronts, and are recognized as an important mechanism in the exchange of heat and salt. The net effects of theses exchanges are becoming increasingly important in higher resolution models, and have been compared (in importance) to those of baroclinic eddies (Ruddick and Richards, 2003a, Joyce et al., 1978). Intrusions can be an essential component of the global cascade of temperature and salinity variances to small scales, providing the link between the lateral stirring by mesoscale eddies and molecular dissipation (Garrett, 1982). Therefore, it behooves the modeling community to accurately parameterize this potential important dynamic driver.

While intrusions can be formed by several different processes (salt fingers, diffusive convection, molecular convection, etc.), this thesis focuses on intrusions driven by salt fingering. Ruddick and Kerr (2003) provide a detailed discussion of the development of intrusions via salt fingering mechanism, which will not be repeated here. Instead, we will provide enough information for a basic understanding of how these intrusions are developed and maintained.

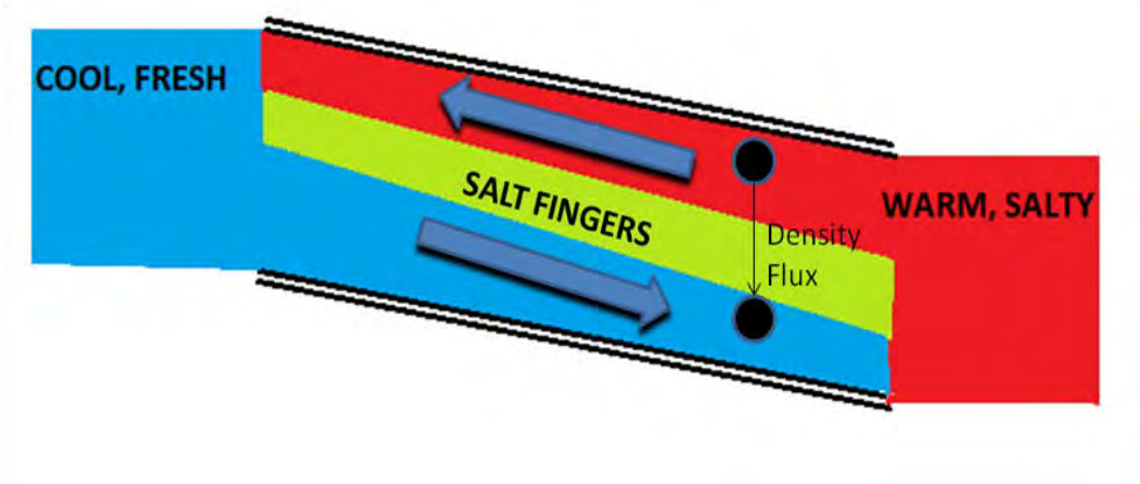

Figure 11. Schematic of a thermohaline front between two water masses. The warm, salty water above cold, fresh creates conditions favorable for salt fingers.

As the two water masses flow over one another, the warm, salty water losses salinity, via salt fingering, to the layer below. The vertical density flux downward (Figure 11) creates a systematic tilt. This tilt, combined with the changes in density, create pressure perturbations that further drive the lateral advective motions. It cannot be over-emphasized that it is the pressure perturbations, and not gravity, that drive the lateral advection, as this tilt is only a fraction of a degree. In other words, further tilting of the intrusion will not accelerate the lateral advections. This positive feedback loop (Figure 12) continues until there is a balance of density gradients.

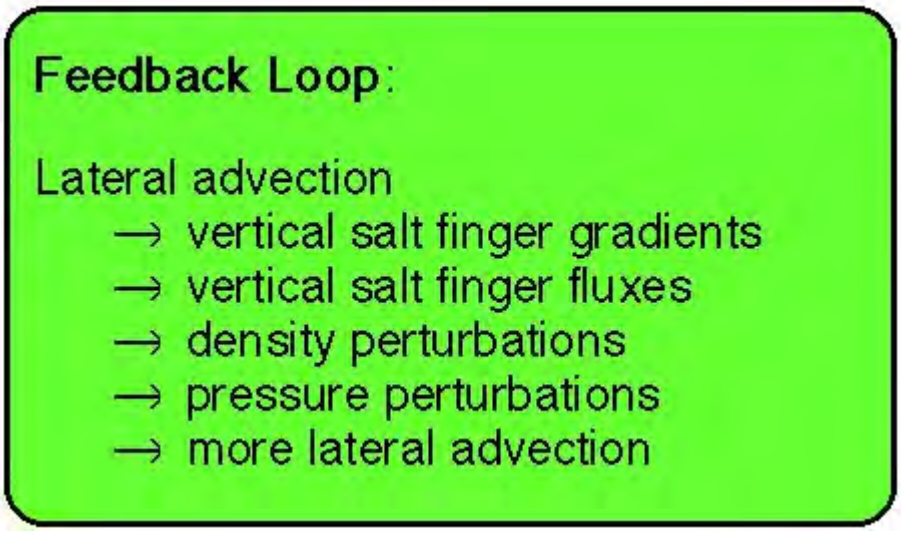

Figure 12. Feedback loop for the evolution of thermohaline intrusions. After Dalhousie University (2011).

It might be useful to explain the development of intrusions from a slightly different point of view. It has been pointed out that the idea of density perturbations leading to pressure perturbations is not physically intuitive. Here, we attempt to demonstrate a step-by-step explanation of the development of thermohaline intrusions. Figure 13 is not to scale, as the distance between the two masses is on the order of several kilometers. Therefore, the angle of the isohalines is greatly exaggerated. The initial environment is of warm, salty water to the right and cold fresh to the left the salinity gradient must in the direction of greater salinity with the isohalines oriented perpendicular to the salinity gradient. If a small perturbation is introduced, it moves warmer, saltier water into a cooler, fresher region, intensifying fingering above layer A and weakening it below. The resulting convergence of salt flux draws salt into layer A. This creates a convergence flow downward in a direction set by the orientation of the initial perturbation. This draws fresher cool water into warmer, saltier water. As a result, the enhanced lateral advections act to enhance the gradient across the interface. This, in turn, makes the salt fingers even more non-uniform, leading to a density convergence. This positive feedback results in the monotonic growth of the intrusion amplitude until it becomes limited by fundamentally nonlinear processes.

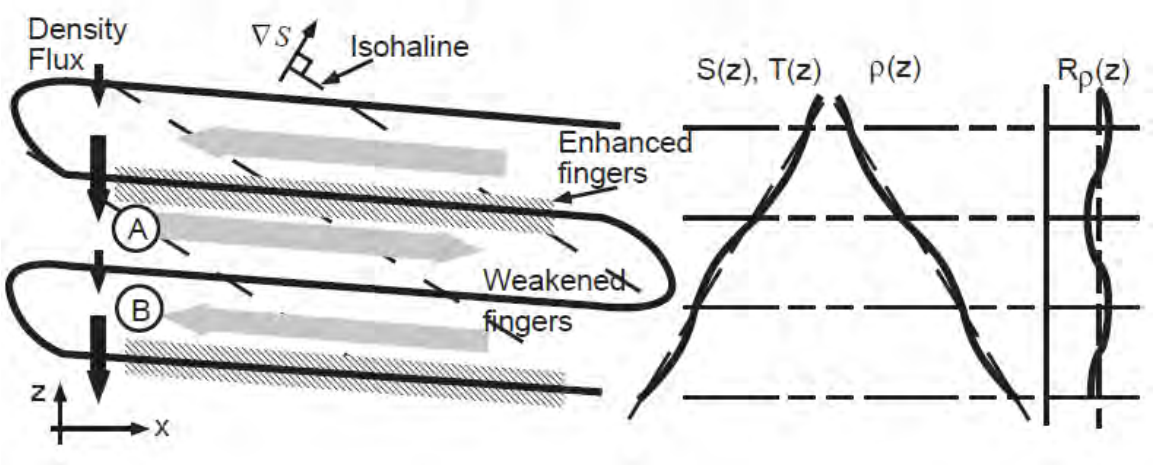

Figure 13. Diagram of thermohaline intrusions. After Simeonov and Stern (2006)

This is by no means a simple problem; one of the main goals of intrusion theory is finding accurate parameterizations for the large and important lateral heat and salinity fluxes, which remains largely unresolved. Accomplishment of this goal requires a clear understanding of the mechanisms responsible for the development of intrusions and their eventual equilibration. It is becoming more important to evaluate the impact of the lateral intrusive mixing on the large- and mesoscale ocean circulation patterns as circulation models resolve sub-mesoscale phenomena. It has been suggested that these thermohaline intrusion provide lateral exchanges comparable in magnitude to mesoscale eddies, thereby significantly influencing the temporal and spatial variability of the ocean circulation (Schmitt, 2003). This signifies that these thermohaline intrusions cannot be ignored in constructing quantitative models of Earth's climate. It is not acceptable to settle for estimations of the bulk effects of intrusions. These small-scale fluxes must be accounted for, quantitatively, in order to incorporate effects of intrusions into most basin scale models.

C. MODELING

Covering nearly three-quarters of the earth's surface, the ocean's role in everything from the geophysical to the socioeconomic is obviously dominant. It is imperative that our ability to understand, model, and predict the ocean's circulation be enhanced so that we can extend our forecasts to anticipate changes. For example,

changes in ocean circulation patterns impact climate variability on the decadal time scales. While it is recognized that these slow changes are imperceptible in the near-time, it is nevertheless important for long-term planning, and with modeling the future can be clearly seen. However, much work needs to be done before the crystal ball of modeling will lift its haze and reveal the true future.

Most modern ocean global circulation models (OGCM) typically have mesh grids with a horizontal resolution of one-hundred kilometers or larger. As a result of this poor resolution, all mesoscale (eddies) and microscale fluxes are subgrid, and therefore their transport effects must be parameterized (Ferrari, 2008). However, with advances in computer systems and processing power increasing at exponential rates, according to Moore's law, it is only a matter of time until models that are capable of resolving scales at the intrusion level become mainstream. Recently, the Hybrid Coordinate Ocean Model (HYCOM) created a 3-dimensional global model capable of 1/12° (approximately 10 kilometers) resolution, although the vertical resolution is still very coarse. There is an expectation that double the resolution, 1/25°, will be achieved by 2013. A 1/25° models of the Gulf of Mexico and the northern section of the Gulf Stream near Newfoundland have already been developed.

Does increasing the resolution show a more accurate picture—and is it worth it? In 2009, Jacobs presented Figure 14 to the Earth Systems Research Laboratory (ESRL). The image compares models of two different resolutions to observed measurements. It is clear that even though there are still errors in the 1/25° model without the data assimilation, it still provides a more accurate representation of the true state, in comparison to the 1/12° model without data assimilation. In particular, it was noted that at the 1/25° resolution, the surface eddy field pumped more energy into the abyssal ocean and the Gulf Stream (Jacobs, 2009). This higher resolution is demonstrating the effects of eddy physics on the circulation. For the purpose of our study, it must be emphasized that the adequate resolution of T–S fronts at the scale of several kilometers opens up an opportunity to incorporate effects of intrusions, albeit in a parameterized form.

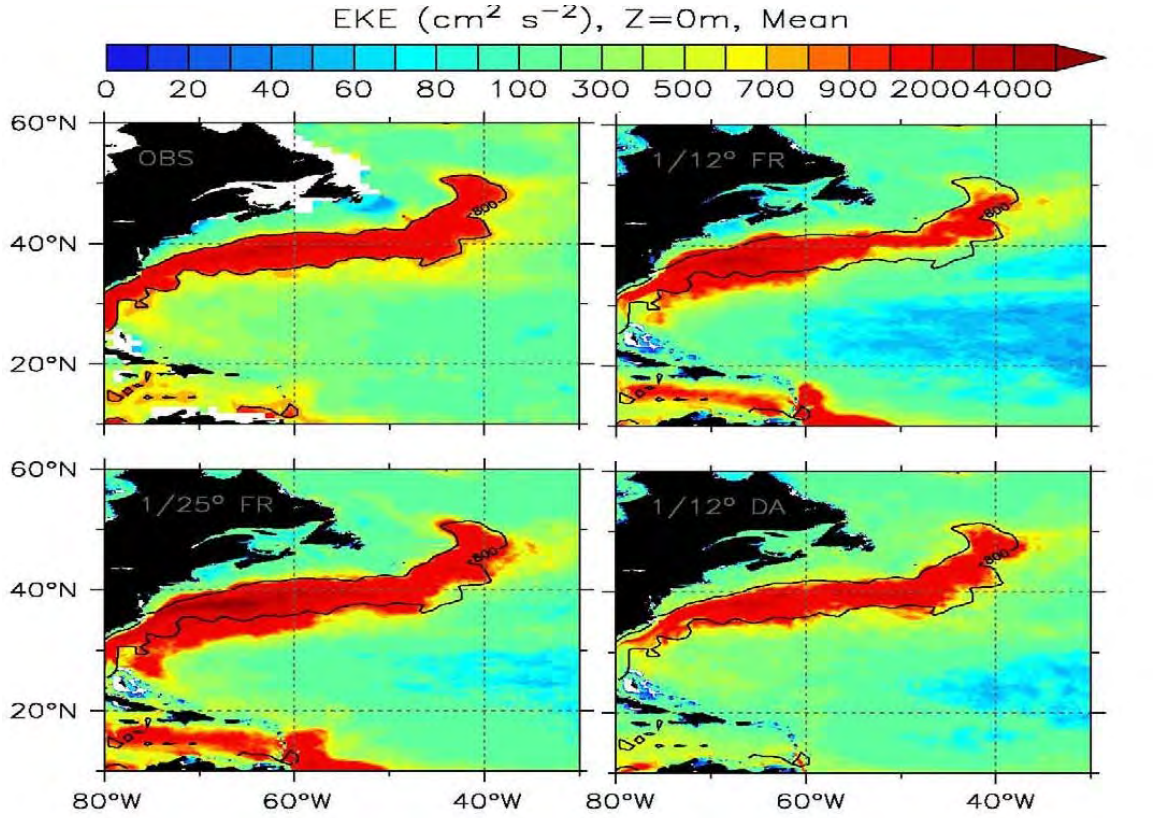

Figure 14. Even if it is not possible in the immediate future to directly account for effects of salt-fingering in our OGCMs, it is feasible to do so indirectly through the development of accurate and physically based parameterizations of salt finger effects on larger scales of modeling. Development of salt finger parameterization, in general, and of thermohaline intrusions in particular is one of the objectives of this thesis.

Preliminary calculations have already been made. Double diffusive processes have been introduced in global models and shown to significantly affect large-scale patterns. In 1998, Zhang investigated the sensitivity of the Geophysical Fluid Dynamic Laboratory's Modular Ocean Model 2 (GFDL MOM2). While still calculating the net effects of double diffusion via crude parameterizations, the study showed that the thermohaline circulations in the model had a greater sensitivity to surface forcing, due to the fact that double diffusion assisted in the generation of self-reinforcing flows. This, in turn, has a greater impact on the meridional overturning and poleward heat transport. Another experiment, utilizing a global ocean model with double diffusive mixing

(Merryfield et al., 1998), demonstrated lesser changes in circulation, but significant regional changes on temperature and salinity.

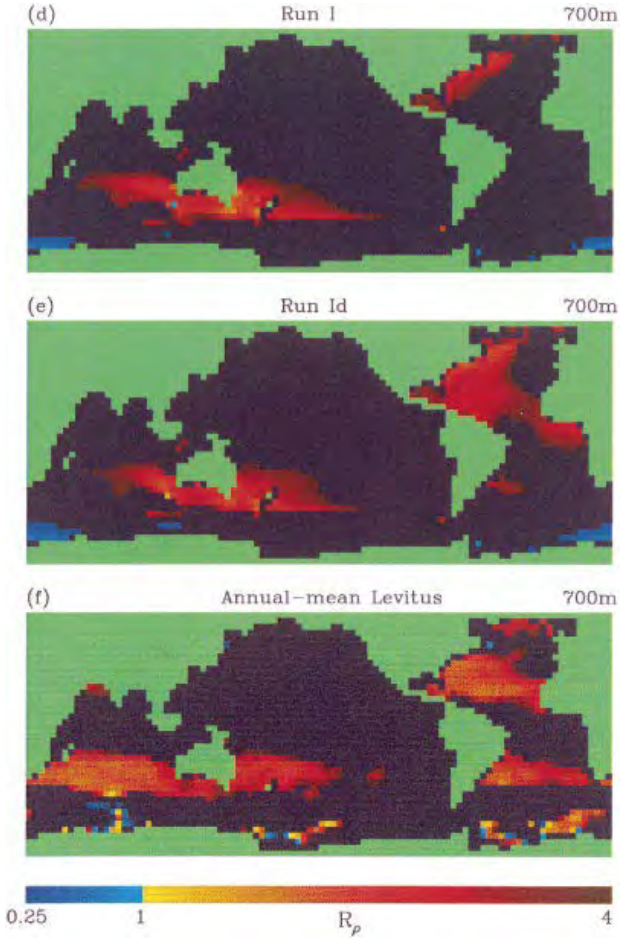

Figure 15. GFDL MOM2. Run1 is run without double diffusion, 1d is with double diffusion, 1f is the annual climatolgical mean from Levitus (1982). Note that double diffusion extends further down into the water column, which implicates importance of double diffusion on meridional circulation. After Merryfield (1998)

D. NUMERICAL MODELING OF INTRUSIONS

In 2006, Simeonov and Stern examined the equilibration of these lateral intrusions, in a doubly-diffusive fluid with uniform unbounded basic-state gradients in temperature and salinity. Previous studies were limited to calculations of growth rates based on parameterizations of small-scale fluxes. Simeonov and Stern avoided uncertainty of existing parameterization by using two-dimensional direct numerical

simulations capable of resolving scales from the smallest fingers to the largest intrusions. Our study differs from Stern and Simeonov in a more comprehensive analysis of all stages of intrusion growth, and in a systematic analysis of the effects of background parameters.

The calculations performed by Stern and Simeonov (2006) kept vertical gradients and the density ratio fixed; they only varied the lateral gradients (G). The experiments presented here vary horizontal gradients (G), density ratio (R_ρ), intrusion angles (θ) and intrusion heights (H) in order to provide a comprehensive account of how changes in background parameters affect the growth, evolution and equilibrium of thermohaline intrusions. A summary of the experiments is provided in Appendix A (Table 1). Additionally, a schematic (Figure 16) is offered to provide the reader a visual reference to each background parameter used in our model.

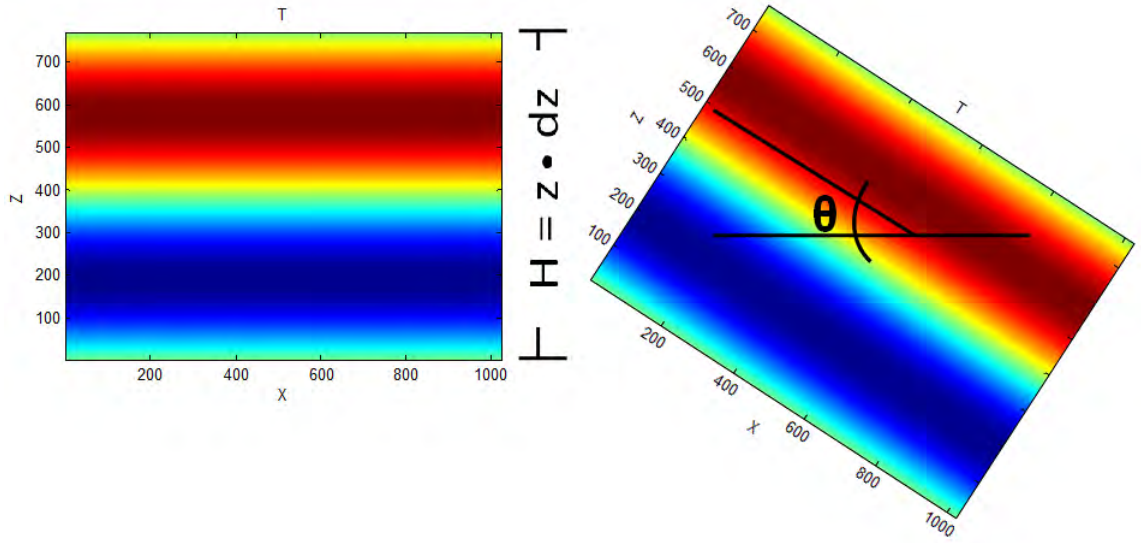

$$G = \alpha \frac{\partial T}{\partial x}, R_\rho = \frac{\alpha T_z}{\beta S_z}$$

Figure 16. Schematic of variables. H = intrusion height, θ = angle of intrusion, G = horizontal gradient and Rρ = density ratio.

E. MEAN FIELD INTRUSION THEORY

We often parameterize in order to include microscale effects in a conceptual model that uses "easier" equations. The term "parameterizations" is used as an assumed substitution of the bulk effects that microscale features have on macroscale processes. In doing so, we are able to model complex dynamics and create a basic understanding of oceanographic processes at work. The small-scale processes can, and often do, present significant impacts on physical processes at much larger scales.

Understanding the limitations that come with using the governing equations is one of the guiding principles behind this research. What if it were possible, however, to incorporate the effects of the microstructure using the actual governing equations without sacrificing computational expense? We would have the perfect solution; but is it possible?

Salt fingering and thermohaline intrusions, as well as many other oceanographic dynamic problems, are analyzed via a method that assumes the vertical fluxes of temperature and salinity due to microscale motion are uniquely determined by the large-scale gradients. This approach is known as Mean Field Theory (MFT) (Traxler et al., 2010); a schematic is shown in Figure 17. This technique models salt fingers, and the fluxes thereby created, via a set of assumed turbulent flux laws. The result is a set of equations that describes the evolution of the large-scale fields only, and can be used to analyze their linear stability. In this context, "large" refers to the intrusion scale and "small" to salt fingers.

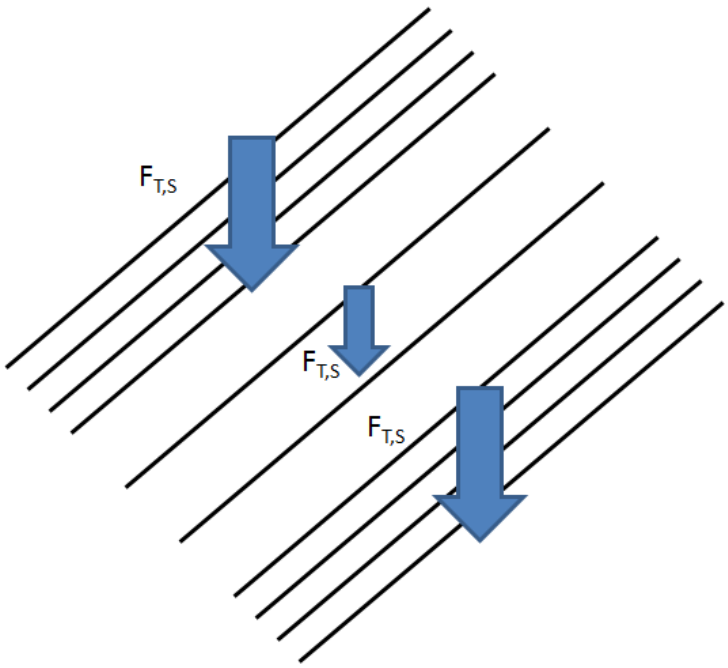

Figure 17. Schematic of Mean Field Theory. Large-scale gradients determine the vertical fluxes of either temperature and salinity noted by subscripts T and S, respectively.

MFT allows one to represent various modes of thermohaline instabilities (i.e., intrusions, collective instabilities, γ -instabilities) via a single mean field system of equations. However, this idea continues to rely on assumed small-scale flux laws. The large-scale temperature and salinity equation in the MFT are given by

$$\frac{\partial T}{\partial t} + Gu + w + \bar{v} \bullet \nabla T = -\frac{\partial F_T}{\partial z} \tag{1}$$

$$\frac{\partial S}{\partial t} + Gu + \frac{1}{R_0} w + \bar{v} \bullet \nabla S = -\frac{\partial F_S}{\partial z}, \tag{2}$$

where (T, S, $\bar{v}$) are the mean field quantities and (F_T, F_S) are the vertical salt finger fluxes.

However, one can readily question the key assumption of MFT, which relates fluxes exclusively to local conditions. The possibility for error in quantifying fluxes lies in the use of this conjecture and flux laws. Testing the accuracy of the mean field theory is one of the objectives of our study.

F. MODULATIONAL STABILITY ANALYSIS

Recent advances in analytical theories have increased our ability to understand dynamics of multiscale systems while reducing the computational effort needed to resolve vastly different scales numerically. One specific example of this has been the perturbation method, which derives averaged equations based on the effects of smaller-scale processes and can be extended to any "random media where the random fluctuations are weaker than the stochastic average" (Mei and Vernescu, 2010).

Mei and Vernescu (2010) call this idea of upscaling from the perturbation to the average, the Theory of Homogenization. We will refer to this theory as Modulational Stability Analysis (MSA). For our purposes, we make use of the fact that salt fingers operate on scales on the order of centimeters whilst intrusions operate on scales on the order of 10's of meters. Such a difference in scales makes the intrusion problem a good candidate for the application of MSA as a tool to describe the long-term evolution of intrusions

Perhaps the easiest way to explain MSA is through an analogy with wave theory. The idea is that we have a rapidly fluctuating process, namely double diffusion, that governs the evolution of the long-term process, thermohaline intrusions. Equation 3 and Figure 18 demonstrate this idea. The slowly varying feature (T) operates on long spatial and slow temporal scales (X,t_{long}) over the entire period, modulated by the rapidly varying feature (orange), which has short period (x, t_{short}).

$$T = \hat{T}(X, t_{long}) \bullet \varphi(x, t_{short}) \tag{3}$$

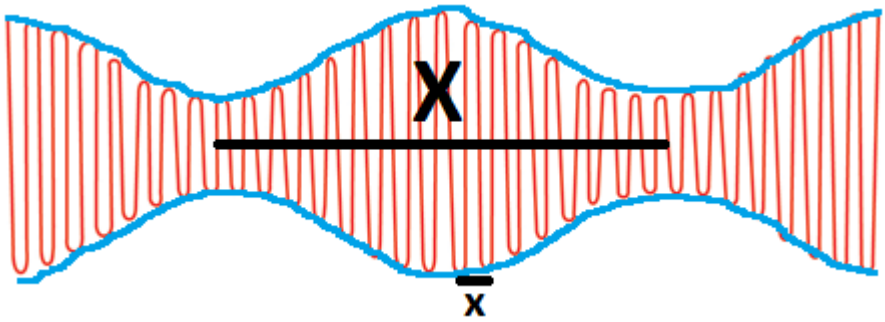

Figure 18. Illustration of Modulational Stability Analysis. Slowly evolving process (blue) is being modulated by rapidly fluctuating process (orange).

The goal of the modulational stability analysis is to formulate a closed set of equations for the modulation component, $\hat{T}$. In comparison to MFT, MSA predicts intrusion characteristics based on two quantities, the microscale temperature variation and individual finger aspect ratio. In doing so, we can directly relate theoretical models to direct measurements from field experiments without involving the assumed parameterizations of vertical fluxes.

THIS PAGE INTENTIONALLY LEFT BLANK

III. METHODOLOGY

Direct numerical simulations were conducted in two dimensions on the Naval Postgraduate School's high-performance cluster, "Hamming." At the time of the experiments, the system was a Sun Microsystems 6048 "blade system" containing 144 blades with 72 nodes and 8 dual-core processors for a total of 1152 cores. It possessed a theoretical peak performance of 10.7 gigaflops. The FORTRAN code was set up for parallel processing using the OpenMP parallelization algorithm allowing for the use of 8 dual-core processors per experiment. Nevertheless, the amount of useable nodes allowed for the possibility of conducting 134 experiments in total.

The numerical model is a fully de-aliased pseudo-spectral model. What this means is that, "all equations are inverted exactly in the Fourier space, and the aliasing error removed by zero-padding" (Radko and Stern, 1999). Integration in time uses the fourth order Runge-Kutta scheme and periodicity in all dimensions. The time-step, used to solve partial differential equations, is limited by the Courant-Friedrichs-Lewy condition (CFL) and computed as a part of the numerical algorithm. In order for the simulation to produce reliable results, the time step must be less than a certain value. The CFL condition for pure advection schemes (one dimension) is given by:

$$\frac{u\Delta t}{\Delta x} < C \tag{4}$$

where C is the Courant number, u, is velocity, Δt time step and Δx is the length interval.

Following Simeonov and Stern (2006), the Navier-Stokes-Boussinesq equations are nondimensionalized by using $d = (g\Theta_z / \kappa_T \nu)^{-1/4}$ for the finger width (length scale), $\mathbf{v} = \kappa_T / d$ as the velocity scale, $\mathbf{t} = d^2 / \kappa_T$ as the time scale, $\mathbf{p} = \nu\kappa_T / d^2$ as the pressure scale and Θ_z , Σ_z as the temperature and salinity scales, respectively. For our experiments, we apply the thermal diffusivity and viscosity for seawater, giving us a Prandtl number of 7. However, due to the size of the domain and limited time, we used a larger salt diffusivity, κ_S, to ease the computational expense. This gives us a diffusivity

ratio of 1/6, which is significantly higher than that of seawater τ=1/100. However, this modification does not alter the fundamental physics and dynamics, but was noted to double the finger fluxes (Radko and Stern, 1999).

The nondimensional Navier-Stokes-Boussinesq equations are modified to the tilted coordinated system (ξ = lateral coordinate, η = vertical coordinate) as follows:

$$\frac{1}{\mathrm{Pr}}\frac{d\vec{v}'}{dt}+\nabla p'=\Delta\vec{v}'+(T'-S')\vec{k} \tag{5}$$

where $\vec{k}=(-\sin\varphi,\cos\varphi)=(-s,1)(1+s^2)^{-1/2}$ is the unit vector anti parallel to gravity and s is the slope.

$$\nabla\bullet\vec{v}'=0 \tag{6}$$

$$\frac{dT'}{dt}+\vec{v}'\bullet\nabla\Theta=\Delta T' \tag{7}$$

$$\frac{dS'}{dt}+\vec{v}'\bullet\nabla\Sigma=\Delta S' \tag{8}$$

$$\frac{d}{dt}=\frac{\partial}{\partial t}+u'\frac{\partial}{\partial\xi}+w'\frac{\partial}{\partial\eta} \tag{9}$$

$$\nabla\equiv\left(\frac{\partial}{\partial\xi},\frac{\partial}{\partial\eta}\right) \tag{10}$$

$$\vec{v}'\equiv(u',w') \tag{11}$$

Equation 12 shows the undistributed nondimensional temperature ($\nabla\Theta$) and salinity ($\nabla\Sigma$) gradients in the tilted reference frame as a function of slope.

$$\begin{aligned}\nabla\Theta&=(a-sR,as+R)R^{-1}(1+s^2)^{-1/2}\\ \nabla\Sigma&=(a-s,as+1)R^{-1}(1+s^2)^{-1/2}\end{aligned} \tag{12}$$

Where $a=\Theta_z/\Sigma_z$ is the tilt of the isohalines. The novelty behind the approach taken is that by tilting the numerical domain we are able to resolve salt fingers on a lateral domain size that no longer has to be on the same order as the horizontal intrusion wavelength. This is important to understand, because with this tilt we would not be able to model these intrusions, since the angle of the intrusions is only a fraction of a degree. The vertical scale of these intrusions is on the order of 10 meters, whereas the horizontal scale is on the order of 100 meters to kilometers. Without placing the coordinate system in the same plane as the intrusions, a box size of 10 meters by 1000+ meters would be required,

making numerical modeling impossible at this time. The idea of tilting the axis appears so simplistic in hindsight, yet it has revolutionized our ability to model intrusions.

THIS PAGE INTENTIONALLY LEFT BLANK

IV. NUMERICAL RESULTS

A. FLOW EVOLUTION

1. Typical Patterns

Under typical conditions, the thermohaline intrusions developed as follows. Figure 19a shows the initial basic state just as intrusion and salt fingers are forming. Movement to the left can be seen in red to the right in blue. Figure 19b occurs shortly after Figure 19a and shows the clear development of salt fingers. Additionally, when we compare the Figures 20a–f we can see they all support the expected dynamics. We see a linear growth in temperature and salinity fluxes, as well as temperature and salinity amplitudes until nondimensional time 1250. After this point, we notice the nonlinear interactions equilibrate all amplitudes as the fluxes oscillate about a mean flux in temperature and salinity. The vertical profile shows two well-mixed layers, with a sharp thermocline and pycnocline at the diffusive interface with less dense water above more dense water, as seen in Figure 20f.

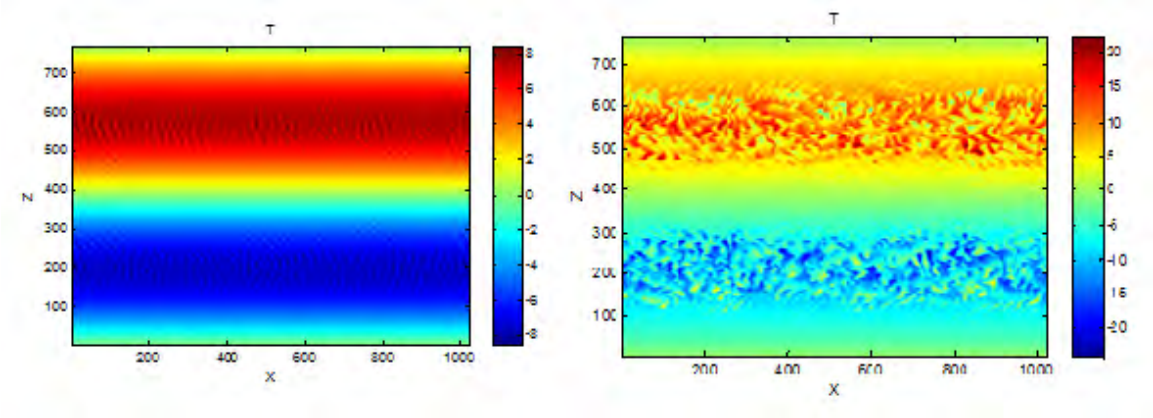

Figure 19. Evolution of temperature field in a typical pattern. (a) Development of intrusions and salt fingering from basic state. (b) Prominent salt fingering developed shortly after Figure 20a.

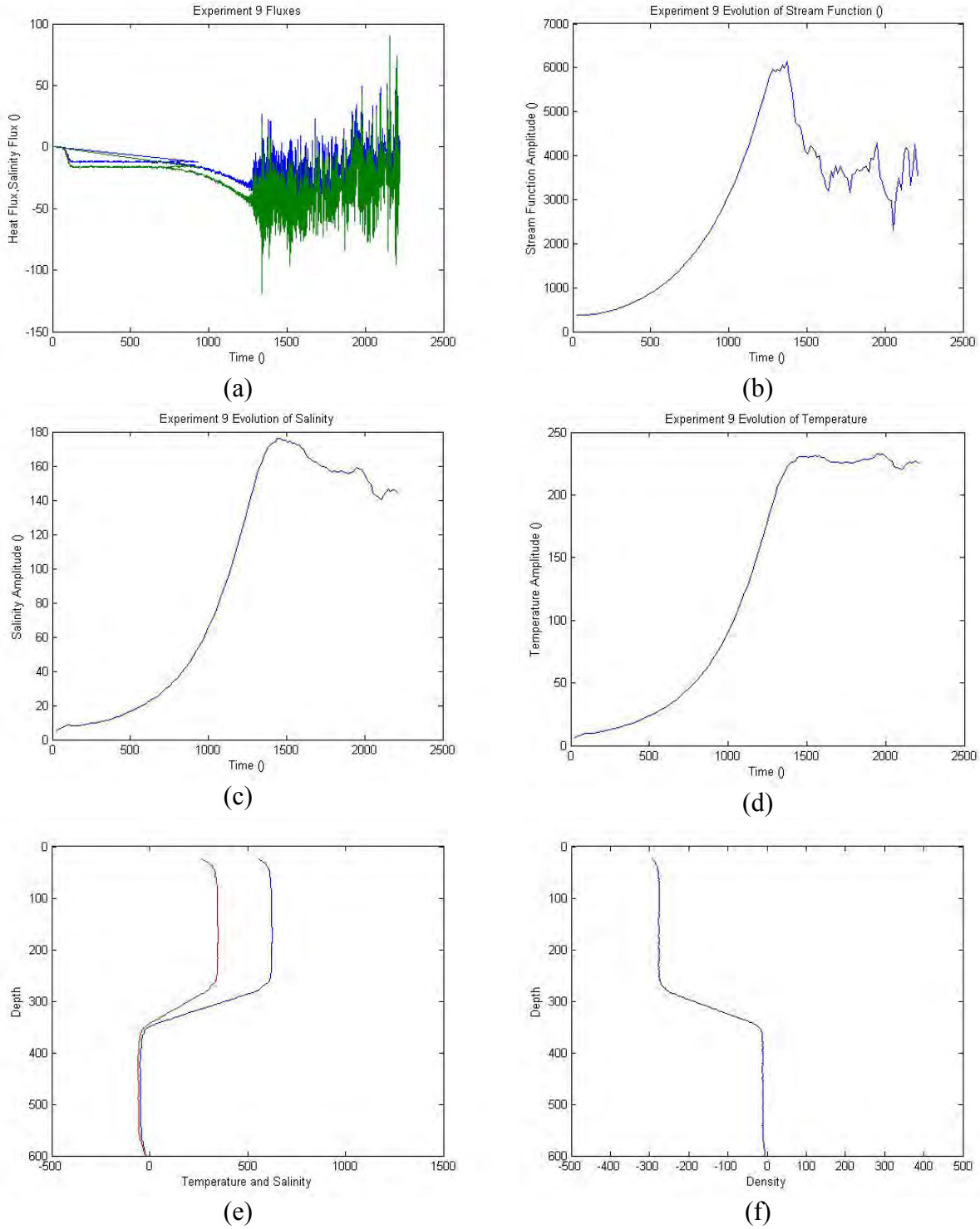

Figure 20. Evolution of thermohaline intrusion. (a) Temperature (blue) and salinity (green) fluxes. (b) Stream function. (c) Salinity and (d) Temperature amplitude in nondimensional time (e) Vertical profile of Temperature (blue) and salinity (red) and (f) Vertical profile of density taken at the end of the experiment.

2. Two-Step Pattern

In addition to the typical pattern, it is important to note another development wherein the diffusive interface begins encroaching from below to develop a second interface. This two-step pattern refers to the two interfaces, salt fingering above and diffusive convection below, that develop. Figure 21a shows the normal development as seen in the typical evolution once intrusions have reached their nonlinear equilibrium. Notice the salt finger interface at $z = 400$. As the experiment progresses, the diffusive interface at the bottom encroaches vertically, reaching approximately z = 250 (Figure 21b). The level of this interface varies between experiments, but the overall pattern remains the same. This pattern develops three clear mixed layers, as seen in Figure 22(b), above and below the salt finger interface as well as below the diffusive interface.

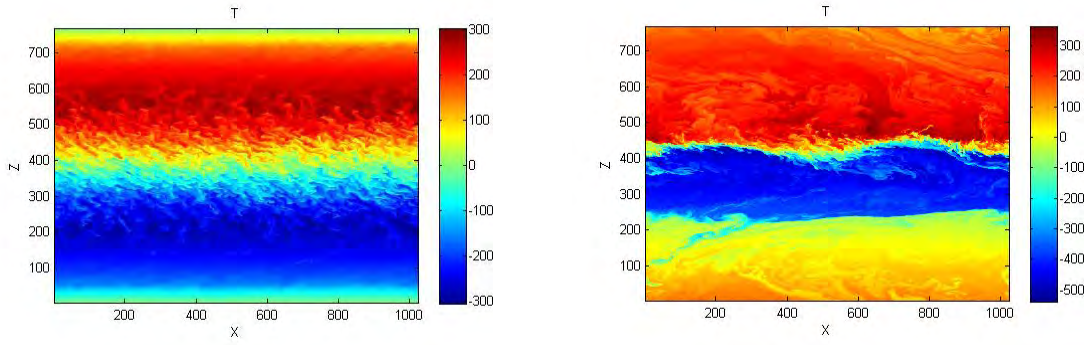

(a) (b)

Figure 21. Evolution of temperature field for a two-step pattern.

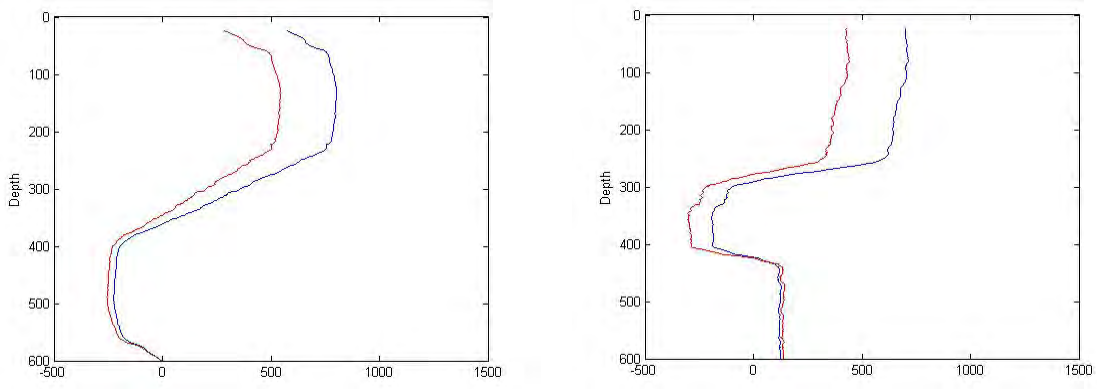

(a) (b)

Figure 22. Vertical profiles of temperature and salinity for Experiment 18. Temperature is blue, salinity is red.

3. Merging Layers

Merging layers are a result of complicated process involving convergences and divergences of heat and salt fluxes. This phenomenon was covered in great detail by Radko (2005, 2007), and is beyond the scope of this thesis. It is interesting to note that this occurs at small angles of intrusions for small density ratios, which intuitively makes sense. However, it is important to note that the intrusions still develop even with the strong vertical fluxes.

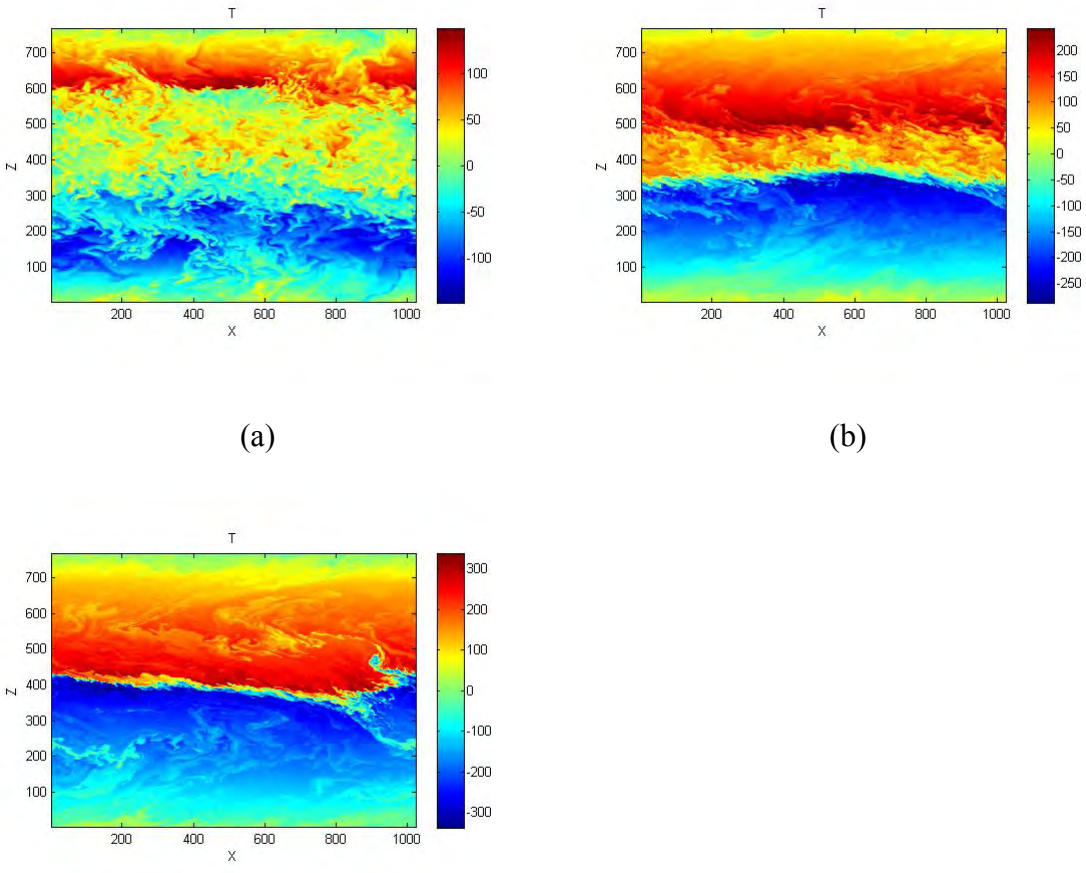

(a) (b)

(c)

Figure 23. Evolution of temperature field for merging layers.

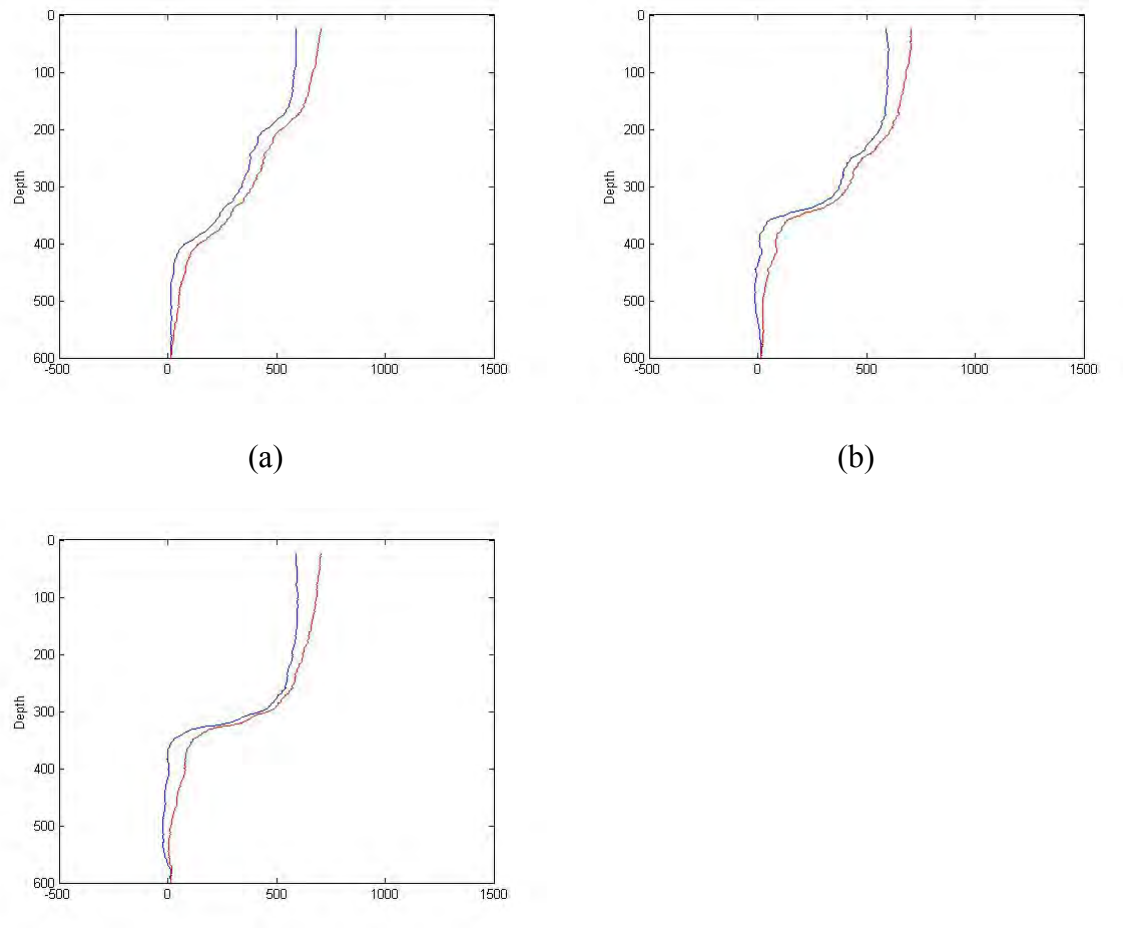

Figure 24. Vertical profiles of temperature and salinity for Experiment 47. Temperature is blue, salinity is red.

4. Kelvin-Helmholtz Instabilities

Analysis of evolutionary patterns realized in numerical experiments revealed a novel phenomenon presenting an exciting new challenge in describing the evolution of thermohaline intrusions. During Experiment 15, we noticed the development of a third mixed layer in between the salt-finger interface. Further investigation led to the realization that the shear due to the opposing intrusion velocities above and below the diffusive interface created Kelvin-Helmholtz (K-H) instabilities, leading to a mixed layer. The new layer appears to have a salt fingering interface at the top and a diffusive

interface at the bottom. Figures (25a–e) show a time progression of the evolution of this phenomenon. In Figure 25d in particular, you can see the classic K-H wave formed near the gridpoint (900,550).

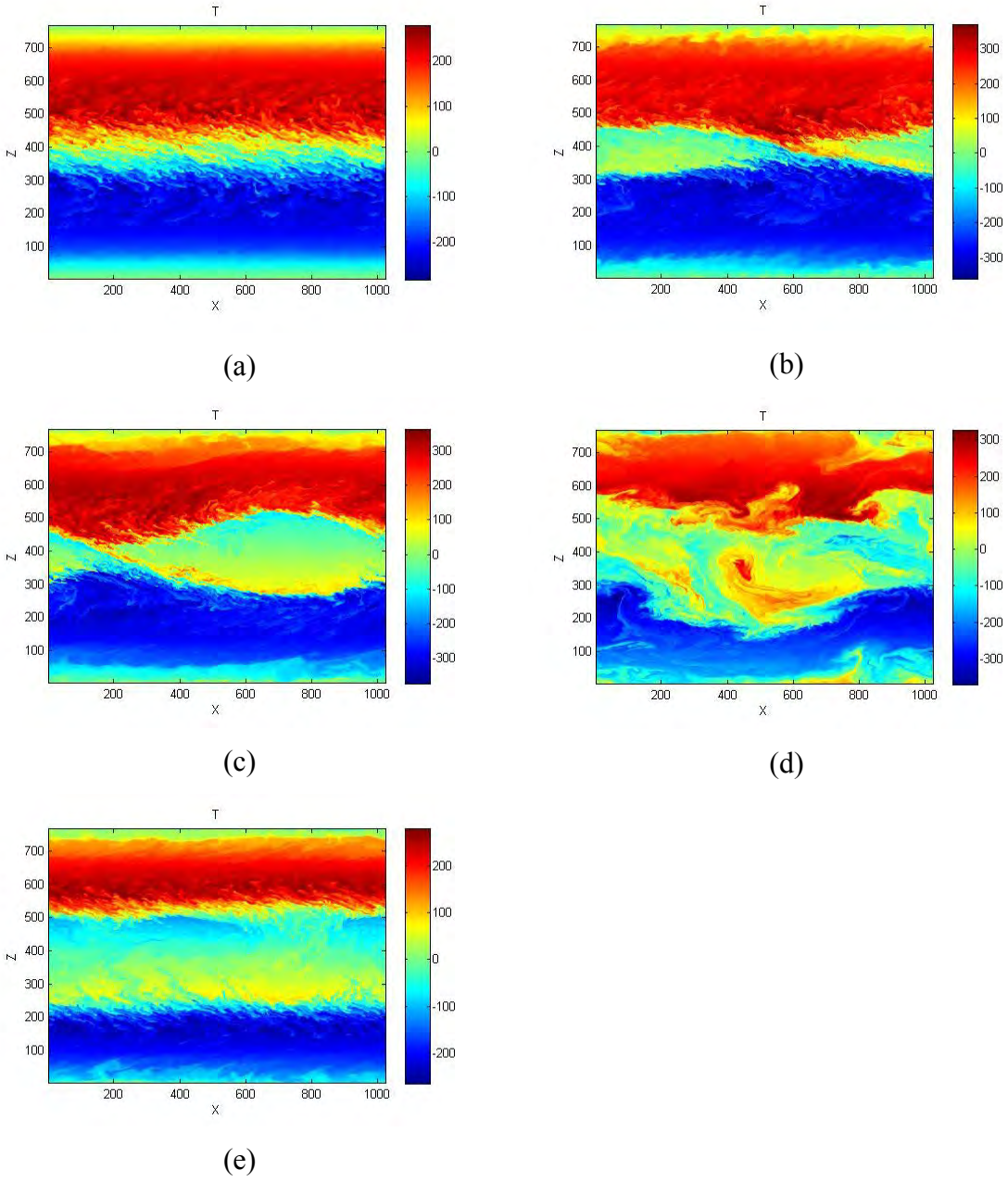

Figure 25. Time progression of the temperature field in an experiment that resulted in the formation of a new mixed layer created by Kelvin-Helmhlotz instabilities.

In addition to the visual detection of the K-H instabilities, we have evaluated instability conditions to ensure that this mixing was indeed the result of K–H instabilities. These instabilities develop the Richardson number (Ri) is less than ¼. In nondimensional units, this results in:

$$Ri = \frac{N^{*2}}{U_z^{*2}} = \frac{\Pr\left(1 - \frac{1}{R_\rho}\right)}{U_z^2}, \tag{14}$$

where R_ρ is the local density ratio and U_z is the local change of velocity, and asterisks denote dimensional variables. The density ratio and shear in the interface were evaluated as

$$R_\rho = \frac{\Delta T}{\Delta S}, U_z = \frac{\Delta u}{h}, \tag{15}$$

where $\Delta T, \Delta S, \Delta u$ refer to variation in properties across the interface. From Figure 26a, when we calculate the Richardson number we receive a value of Ri = .06, which is significantly less than the dynamical instability criteria, supporting our initial hypothesis that this are Kelvin-Helmholtz waves.

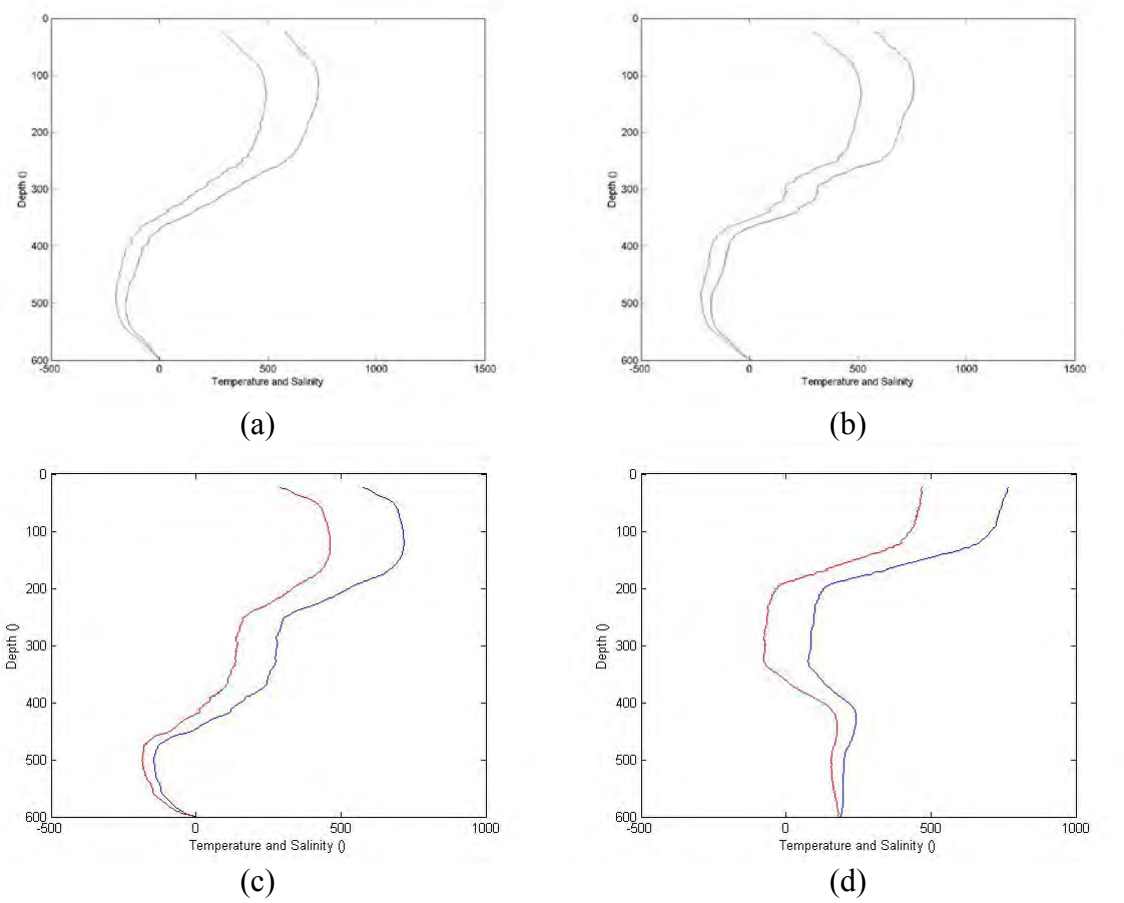

Figure 26. Vertical profiles of temperature and salinity for Experiment 15. Temperature is blue, salinity is red.

5. Summary of the Observed Patterns

In trying to conclude the results from our observations, it is helpful in plotting the different evolutions based on the parameter space. Figure 27 presents that schematic to show specific regions of how the patterns develop in the parameter space. This may be useful in providing parameter controls for later use in models. Based on the numerous and very different dynamics, it may prove prudent to develop boundaries to provide the most accurate parameterization for future models.

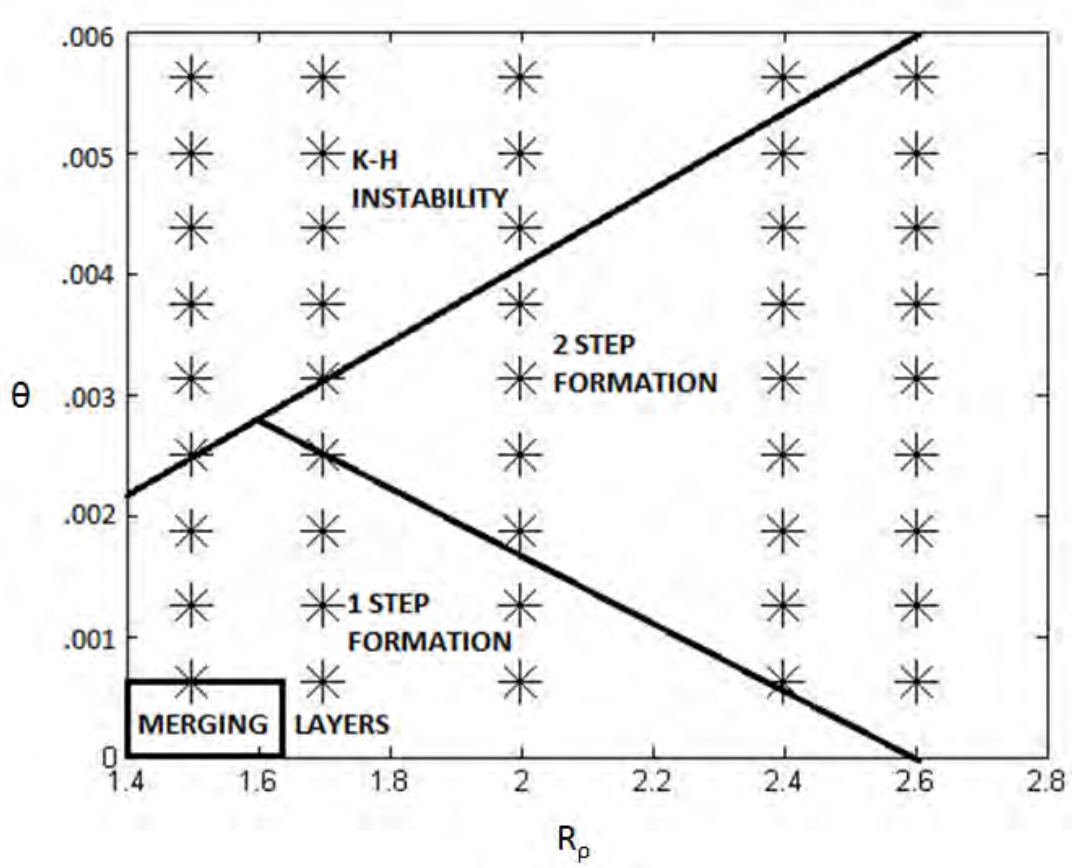

Figure 27. Evolutions of vertical profiles for varying density ratios (x-axis) and θ (y-axis).

B. GROWTH RATES

In the ocean, there are numerous perturbations. Naturally, these perturbations will compete for dominance in controlling thermohaline intrusions and the one with maximum growth rate will control the dynamics. Therefore, it is suggested that intrusions will favor the slope with the maximum growth rate. Therefore, it is important for us to understand how the background parameters affect these growth rates.

In Figures 28a–d, we have plotted growth rates as a function of the four different background parameters, in order to give a clear understanding of how each one affects the growth of the intrusions. As we can see from Figures 28a and 28d, intrusions have an optimum growth rate at a defined maximum angle. As the density ratio decreases the maximum intrusion angle and growth rate increases. This makes sense, as low density ratios support more salt fingering. Salt fingering, in turn, increases the systematic tilt of

the intrusion due to the more rapid exchange of salinity. Figure 28b appears to be linear, however, when fitted with an exponential best fit line, which suggests that growth rates as a function of density ratio are indeed exponentially decreasing. The undulations with different density ratios are actually small when compared to the overall variation in density ratios. Figure 28c shows a nice exponential, as might be expected, because at a certain point there can only be so much lateral transport regardless of the lateral differences.

From Figure 28d, it is tempting to conclude that an increase in H will lead to faster growth rates, but it is presumptuous to state that conclusion as fact. Attempts were made to model the effects of H = 1000; however, the experiment proved too computationally taxing and did not reach equilibrium in the allotted time frame. Theory would suggest that there is a maximum H allowable.

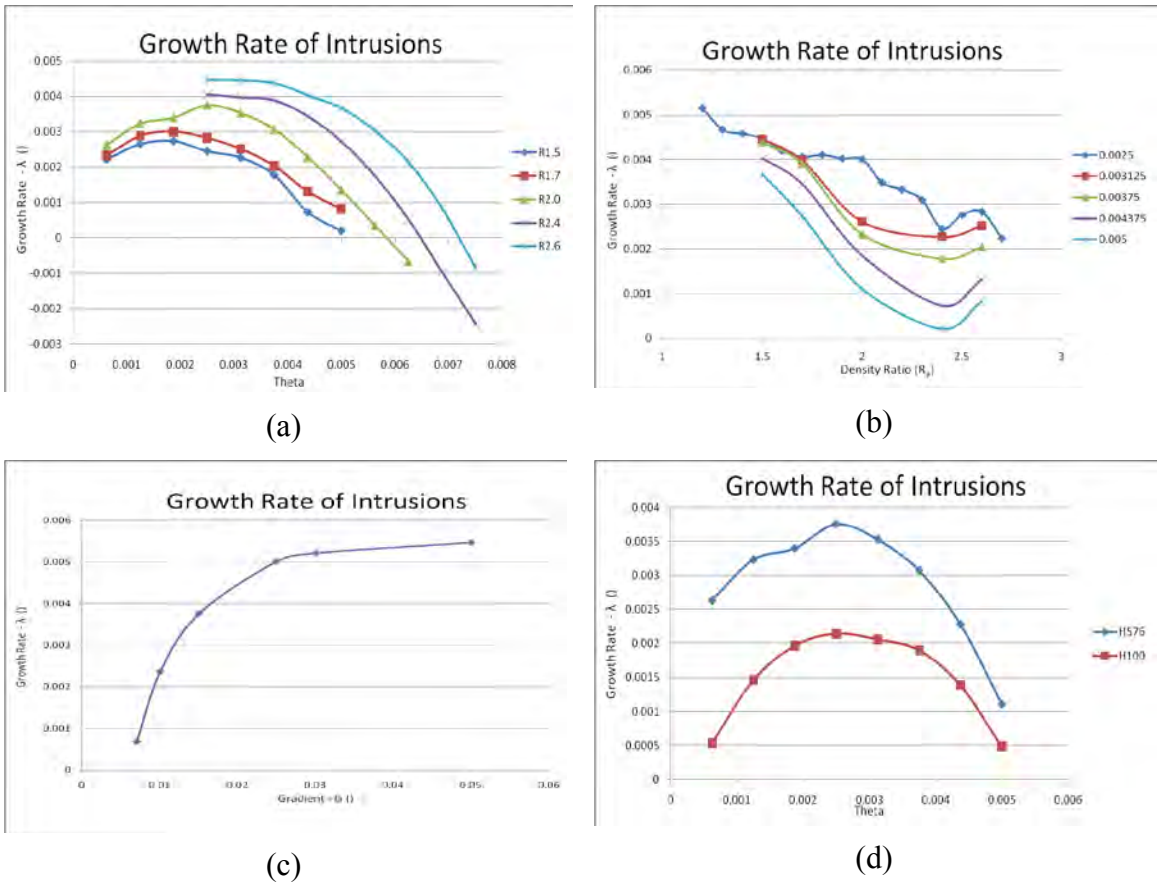

Figure 28. Growth rates of intrusions as a function of theta and density ratio. Growth rates are in nondimensional units.

C. INTER-COMPARISON OF THEORIES AND NUMERICAL SIMULATIONS

The assessment of theoretical models was made by comparing their prediction of growth rate with numerical simulations. As we can see in Figure 29, the mean field theory surpasses the modulation stability analysis in terms of matching numerical growth rates. It is also clear that MFT is also insufficiently accurate at predicting growth rates at lower density ratios (Figure 30a and b). This is very important to note; many areas of the ocean experience density ratios of less than 2.0, especially near the equator, where there is strong evaporation as a result of the consistent solar radiation. Figure 31 shows the distribution of density ratios in the North Atlantic.

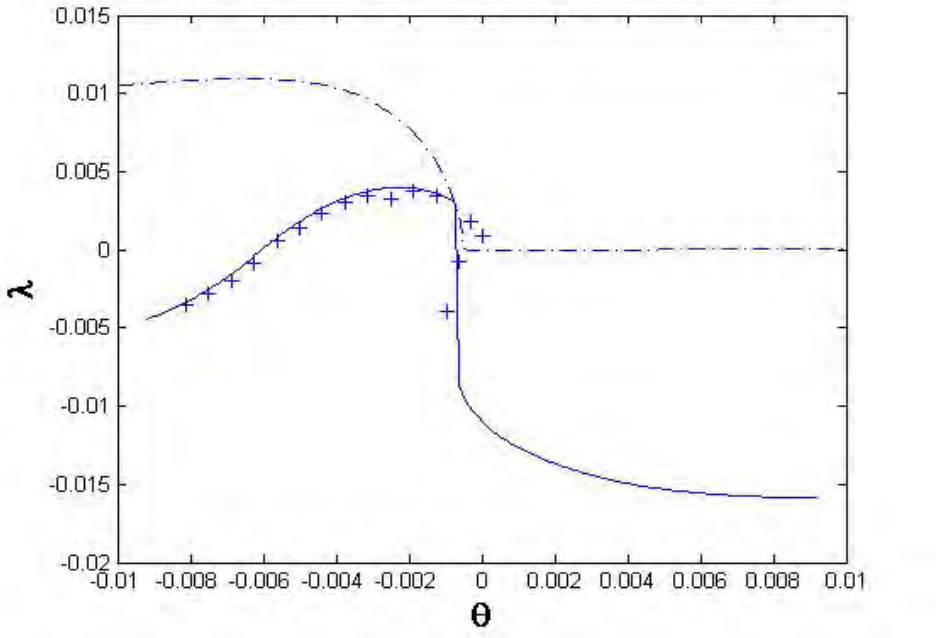

Figure 29. Comparison of MSA (dashed blue line) predicted growth rates with observed growth rates from model (crosses) and MFT (solid blue line) for Rρ=2.0.

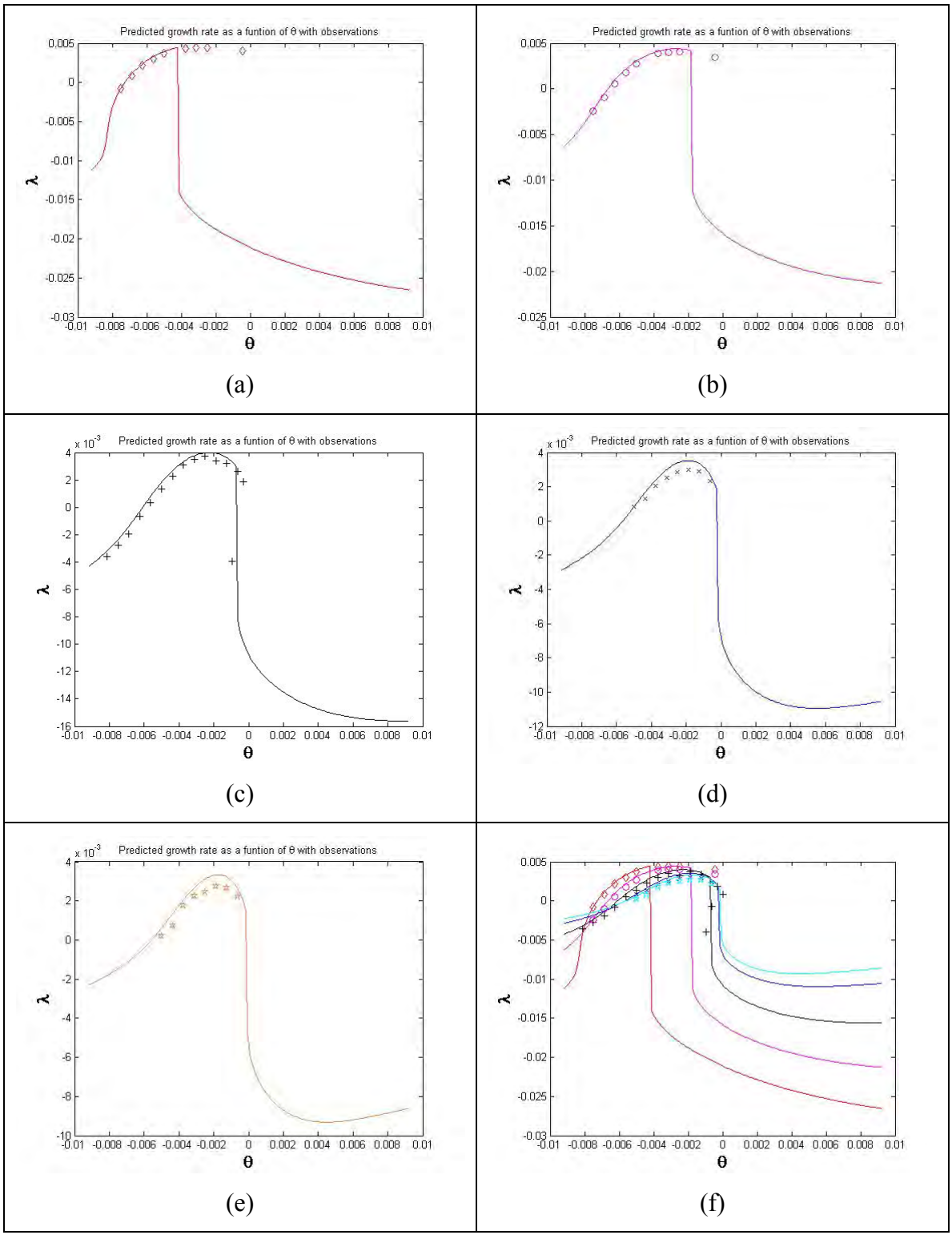

Figure 30. Comparison of MFT predicted growth rates with observed growth rates from model for (a) Rρ=1.5–(e) Rρ=2.6. Combined MFT predicted growth rates from Rρ=1.5–(e) Rρ=2.6 (f).

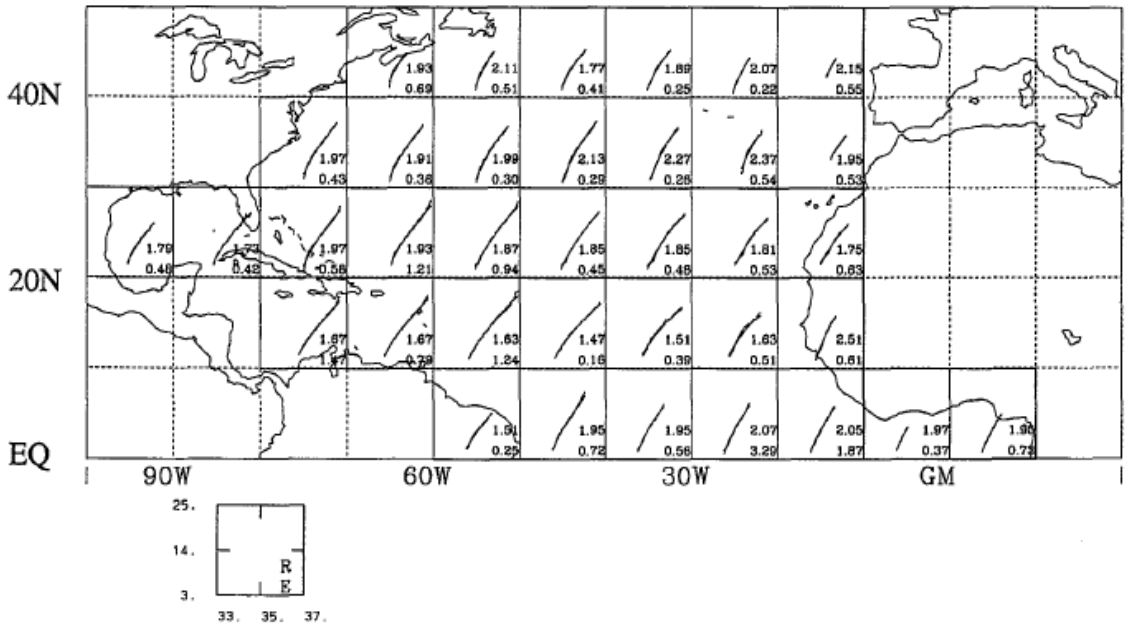

Figure 31. North Atlantic density ratios. The upper and lower numbers in the lower right hand corner of each box refer to the density ratio and error, respectively. After Figueroa (1995)

D. NONLINEAR EQUILIBRIUM REGIME AND DIFFUSIVITIES OF HEAT AND SALT

What is perhaps the most important contribution of this research is the estimate of eddy diffusivities due to intrusions. Since this process is, for the most part, subgrid, we can only account for its effects on the dynamics of a model through fluxes of temperature and salinity. These fluxes are a function of eddy diffusivities (κ), which in turn are a function of θ, R_ρ, G, and H.

$$F_{T_{Horizontal}} = \kappa_{T_{Horizontal}} \frac{\partial T}{\partial x}, F_{T_{Vertical}} = \kappa_{T_{Vertical}} \frac{\partial T}{\partial z} \tag{16}$$

$$F_{S_{Horizontal}} = \kappa_{S_{Horizontal}} \frac{\partial S}{\partial x}, F_{S_{Vertical}} = \kappa_{S_{Vertical}} \frac{\partial S}{\partial z} \tag{17}$$

It is very difficult to determine a unique equation that simultaneously solves the variability of κ when it is a function of multiple parameters. Our ultimate goal, then, is to look at how each individual parameter affects the eddy diffusivities and attempt to describe the eddy diffusivities as a function of all the parameters. These parameterized diffusivities can then become incorporated into models to enhance their skill.

$$\begin{aligned} \kappa_{T_{Horizontal}} &= f(R_\rho, \theta, G, H), \kappa_{T_{Vertical}} = f(R_\rho, \theta, G, H) \\ \kappa_{S_{Horizontal}} &= f(R_\rho, \theta, G, H), \kappa_{S_{Vertical}} = f(R_\rho, \theta, G, H) \end{aligned} \tag{18}$$

As a function of θ the calculated eddy diffusivities produced nice polynomial curves with a specific peak, confirming that at the maximum growth rate there is a maximum of both lateral and vertical mixing. As seen with growth rates, the maximum of eddy diffusivities shifts toward higher angles for lower density ratios. The overall eddy diffusivities are much higher horizontally. There appears to be an anomalous change in eddy diffusivities for the density ratio of 2.0. The reason is tentatively attributed to a unique combination of parameters, which creates the most favorable conditions for intrusions, allowing for the higher diffusivities at this specific density ratio.

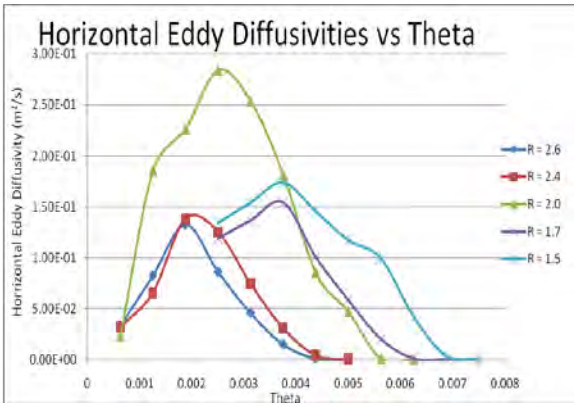

(a)

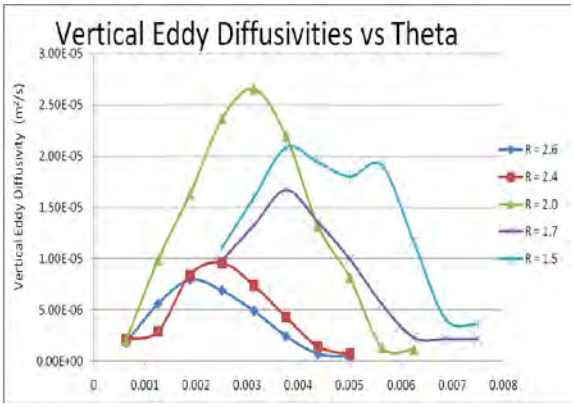

(b)

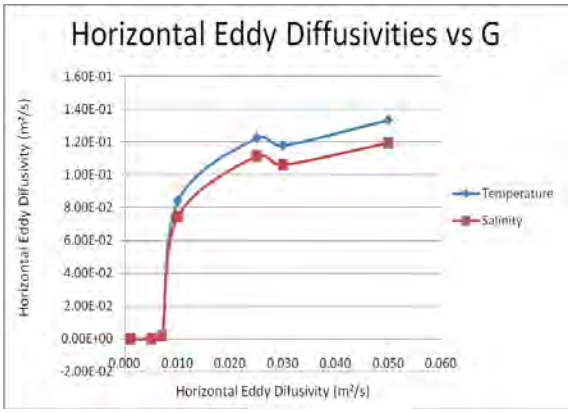

(c)

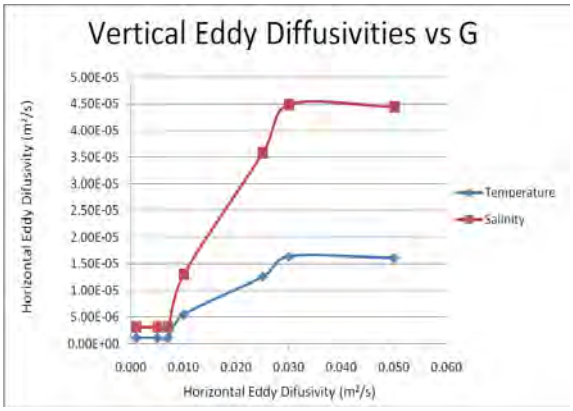

(d)

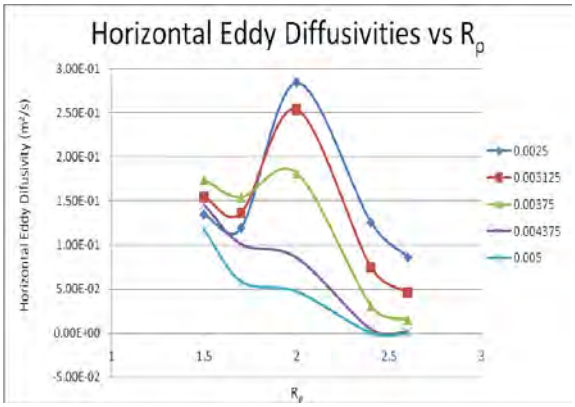

(e)

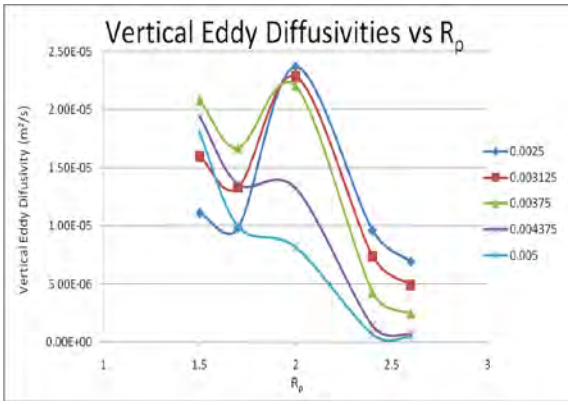

(f)

Figure 32. Eddy diffusivities for varying parameters.

Figures 32c–d show the horizontal and vertical diffusivities as a function of horizontal gradient, G for a fixed density ratio of 2.0 at its maximum intrusion angle. While it would have been prudent to conduct more experiments varying both G and R_ρ, as intrusions are a process affected by lateral differences, the time constraints and available resources simply did not allow it. Nevertheless, we see a clear logarithmic growth for similar reasons that we saw for growth rates, λ.

E. PROPOSED PARAMETRIZATION ALGORITHM

We have examined how several background parameters affect the evolution of intrusions, the resulting growth rates and eddy diffusivities. However, it is more important to be able to incorporate this knowledge into quantitative results that could be used for modeling. Since we are 20 years or more from obtaining global models that are capable of resolving these intrusions, it is important that we develop accurate parameterizations. Since the investigation in the change of parameters did not yield an explicit analytical expression for the intrusive fluxes of temperature and salinity, we propose the following parameterization algorithm to be tested in the future. Figure 33 provides a schematic of the algorithm.

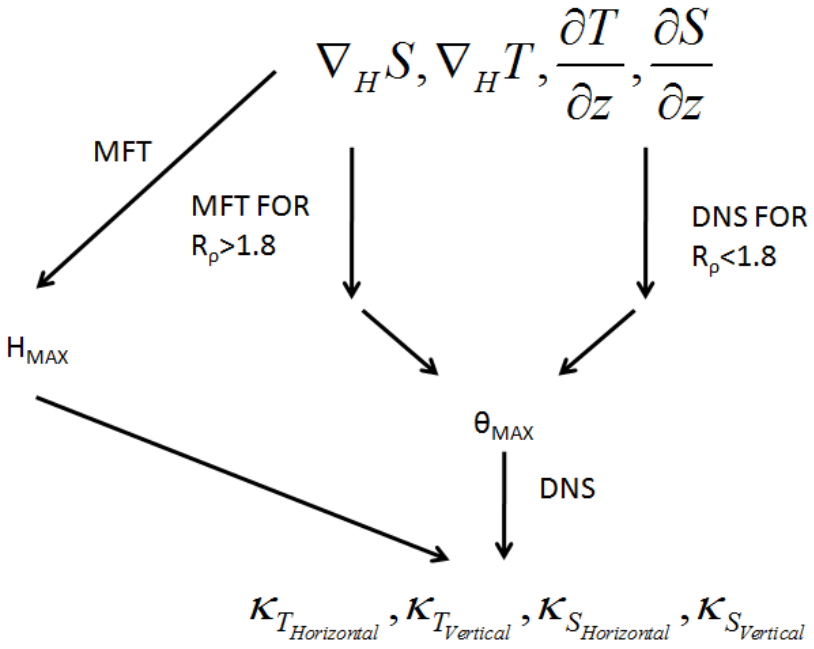

Figure 33. Schematic of the proposed parameterization algorithm.

Given:

$$\nabla_H S, \nabla_H T, \frac{\partial T}{\partial z}, \frac{\partial S}{\partial z},$$

where $\nabla_H S, \nabla_H T$ are the horizontal gradients of temperature and salinity, respectively and $\partial T/\partial z, \partial S/\partial z$ are the temperature and salinity gradients in the vertical, we may be able to provide some input for eddy diffusivities. These gradients can be measured in the field and are readily available in models. We can then calculate θ_{MAX} , which we have shown provides the most likely eddy diffusivity values for intrusions. Using MFT for density ratio greater than 1.8 provides an accurate estimate of θ_{MAX} ; for R_ρ , less than 1.8 tabulated results of direct numerical simulations would be required. The second step involves using the tabulated results of numerical simulations such as ours, which would provide an accurate estimation of the eddy diffusivities as a function of H_{MAX} and θ_{MAX} evaluated in step 1. The final result is an accurate representation of thermohaline intrusions in large-scale models.

THIS PAGE INTENTIONALLY LEFT BLANK

V. DISCUSSION

A. CONCLUSIONS

Previous studies have fallen short by not investigating how background parameters affect the evolution of thermohaline intrusions. One of the objectives of this study was to determine the utility and relative merits of leading theoretical models of intrusions. The numerical simulations were made possible by using the tilted coordinate system, which dramatically reduces the computational effort. From our data, we have shown that Mean Field Theory appears to be superior Modulational Stability Analysis in predicting the growth rates of thermohaline intrusions. However, as successful as Mean Field Theory was in predicting growth rates, the theory becomes inaccurate in predicting the dependence of the growth rate on slope when density ratios are less the 1.8. This precludes usage of MFT in practical applications at low R_ρ. The lack of accuracy at lower density ratio necessitates either the use of computers, which can be prohibitive in time and resources, or requires a new theory to be developed.

By examining the evolution of thermohaline intrusions and resulting eddy diffusivities, we have been able to determine how each parameter individually affects the growth of intrusions. However, results from investigation leave questions about whether the physical combination of parameters, which may have interdependencies of their own, might be more important in explaining the nonlinear interactions of thermohaline intrusions. One of the key recommendations of this study is a proposed parameterization algorithm, which connects the eddy diffusivities due to intrusions with background gradients, and which could potentially be entered into global models. While we recognize some shortcomings from the lack of experiments conducted, this is a first step in trying to bring the effects of thermohaline intrusions into models.

It is important also to recognize that this research has demonstrated very rich behaviors in the development of thermohaline intrusions. The development of secondary

effects, such as Kelvin-Helmoholtz instabilities and the interfacial drift or merging layers, offers unique case studies to further our understanding of the development of an accurate parameterization of thermohaline intrusions.

B. NAVAL IMPACTS

In 1986, Rear Admiral J.R. Seesholtz, then Oceanographer of the Navy, stated that he wanted the U.S. Navy to "develop a Global Ocean forecasting capability" (Peloquin, 1992). The U.S. Navy's current ocean modeling capabilities were formed from this simple statement as the oceanographer then acquired the first of two Cray YMP supercomputers, capable of 333 megaFLOPS. The primary objective of giving the U.S. Navy a modeling capability was "to produce three-dimensional environmental data fields for assessing and predicting the performance of operational systems" (Peloquin, 1992). In less than 20 years, the U.S. Navy has significantly advanced, and currently possesses several supercomputers, of which the most advanced is a Cray XT5 supercomputer, "Einstein," capable of 1.3 petaFLOPS on 2045 cores with plans to upgrade to machines with 40K–60K cores for fiscal year (FY) 2013.

By having an understanding of the histories behind thermohaline intrusions and the Navy's current computer modeling capabilities, one can begin to develop the insight toward what science is currently capable of and where the future lies. Advances in research and computing are collectively pushing toward higher resolution models with numerous complex physical interactions. The ocean's size, environment and timescales make it extremely difficult to collect observations and make predictions based on limited collected data. The U.S. Navy's global presence in an unpredictable world makes it impossible to focus collections in specific geographic regions. Therefore, naval ocean forecasting must be a compromise between what is possible and what is operationally practical. What drives the Navy's decisions on where and what topics to research? In 2002, the National Military Strategy had three principle concerns that operational oceanography must support: 1) engagement during peacetime, 2) deterrence and prevention of conflict, and 3) fighting and winning wars when necessary (Burnett and Harding, 2002).

From the modest objective of simply assessing and predicting the performance of operational platforms, the Meteorology and Oceanography (METOC) community has continually transformed to meet tomorrow's challenges. METOC supports the National Military Strategy tenets through "Battlespace on Demand" (BonD) (Figure 34), which is a four-tiered construct. The bottom tier is the collection of environmental data, which is used by models to produce forecasts. These forecasts are then analyzed and presented to the customer in a format that best assimilates the forecasts with other factors, measurable and immeasurable, so that the operator can pull out the most important information quickly and clearly. This leads to the top tier where decisions are made. As can be seen from the pyramid, each tier builds upon the previous; if the foundation of any is inadequate, the ultimate result is a flawed decision.

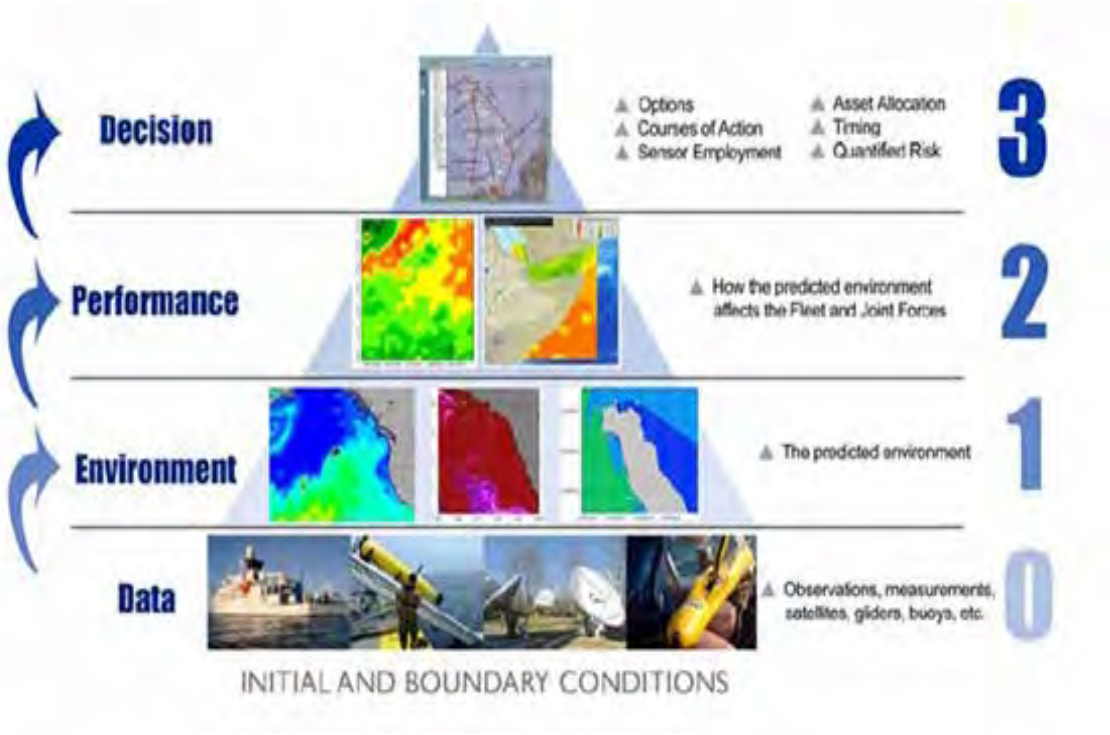

Figure 34. BonD pyramid.

This entire cycle repeats for changes in times, new observations, and new information. Figure 35 demonstrates just how complex this cycle can be for naval oceanography. The global models provide initial conditions for regional models. The regional models then feed their output to on-scene models, which assemble on-scene

observations, producing the NOWCAST. In-area changes can be updated in the NOWCAST within 0–2 hours to provide the most up-to-date information from which to develop the "battlespace awareness cube." This allows decision-makers to process their environment effectively and efficiently. This "nesting" of higher resolution regional models within the global model provides some reduction in response time to these changes. However, any improvements to the models will only improve information provided to decision-makers for most accurate and up-to-date information.

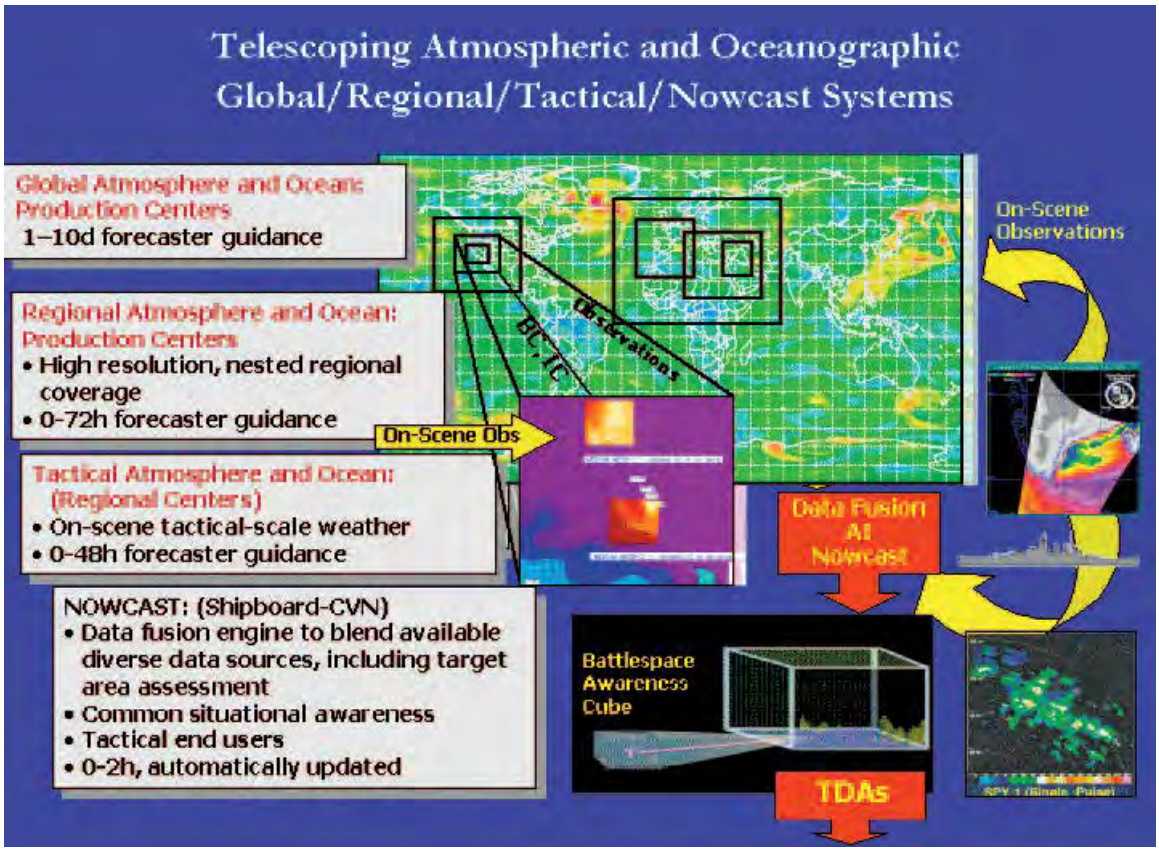

Figure 35. BonD loop. After Burnett and Harding (2002)

As of 2002, the Office of Naval Research (ONR) and the Oceanographer have set forth that Research and Development (R&D) investments must focus on 1) Data—the ability to collect environmental data (Tier 0), 2) Information—the ability to assimilate observations in to the highest resolution models (Tier 1), and 3) Knowledge—the ability to characterize and predict the environment and its impacts on "people, marine life,

weapons, sensors and platforms" (Tiers 2 & 3) (Burnett and Harding, 2002). This research addressed two of the three key areas (Information and Knowledge) by providing an explicit parameterization.

This research addressed all of the aforementioned tiers except for the first. Even so, by addressing tier 1 through tier 3, this research also directly supports the three tenets of the National Military Strategy.

THIS PAGE INTENTIONALLY LEFT BLANK

VI. RECOMMENDATIONS FOR FUTURE RESEARCH

Our preliminary model-based estimates of growth rate and slope of intrusions are encouraging in terms of qualitative consistency with observations and laboratory experiments. It is also encouraging that we were able to provide qualitative measurements for eddy diffusivities and to propose a parameterization algorithm for the effects of thermohaline intrusions. However, we readily admit that our model is highly idealized and excludes a number of important elements, such as three-dimensional dynamics, baroclinicity, frontal spreading, etc. Therefore, it is our recommendation that these experiments be conducted in a three-dimensional environment in order to compare the potential differences in magnitudes of eddy diffusivities.

While many of the experiments were run for some time in the nonlinear equilibrium state, others were not. Therefore, these experiments could be run for longer durations in order to examine the confidence interval for the value of the calculated fluxes, providing the end user with additional assurance in the accuracy of these values. Ideally, more experiments to examine how the diffusivities change as a function of G for several different R_ρ and θ should be conducted. This will provide an improved constant for the effects of G. Additionally, more experiments with varying H might prove to be helpful, as very little was gained from the experiments conducted in this research.

Finally, some of the more interesting cases should be pursued as case studies. The idea of Kelvin-Helmholtz instabilities developing in nonlinear intrusions is a new and exciting avenue to explore.

THIS PAGE INTENTIONALLY LEFT BLANK

APPENDIX A.

Table 1. Summary of background variables changed in all experiments. Amplitude remains the same all experiments after Experiment 9. With and without initial wave perturbation refers to a sinusoidal wave imposed over the uniform and random T-S fields at initialization

EXPERIMENTS	**R_ρ**	**G**	**H**	θ	**OTHER CHANGE**
1–8	2	.015	576	.000625–.005	None
9–23	2	.015	576	.0003125–.0075	Amplitude
24–30	2	.015	576	-.000625–(-.005)	Amplitude
31–46	1.2–2.7	.015	576	0	With Initial Perturbation
47–58	1.2–2.7	.015	576	.0025	Without Initial Perturbation
59–90	1.5–2.6	.015	576	.00625–.005	With Initial Perturbation
91–97	2	.001-.05	576	.0025	None
98–103	2	.001-.05	576	0	With Initial Perturbation
104–107	2	.01-.05	576	0	Without Initial Perturbation
108	2	.015	100	0	With Initial Perturbation
109	2	.015	100	0	Without Initial Perturbation

110	2	.015	1000	0	With Initial Perturbation
111	2	.015	1000	0	Without Initial Perturbation
112–119	2	.015	100	.000625–.005	None
120–127	2	.015	1000	.000625–.005	None
128,129	2	.015	205	.0025,.004375	τ=.001
130,131	2	.015	410	.0025,.004375	τ=.001
132	2	.015	150	.0025	None
133	2	.015	750	.0025	None
134	2	.00375	576	.0025	None
135	2	.01875	576	.0025	None

APPENDIX B.

Table 2. Table of values calculated for experiments.

Experiment	Background Parameters	$K_{T\text{-Horizontal}}$ $K_{S\text{-Horizontal}}$	$K_{T\text{-Vertical}}$ $K_{S\text{-Vertical}}$	Growth Rate (λ)
9	$R_\rho = 2$, G = .015, H = 576, θ = .000625	2.28E-02 2.022E-06	1.61E-02 5.974E-06	0.002633
10	$R_\rho = 2$, G = .015, H = 576, θ = .000125	1.86E-01 9.883E-06	1.57E-01 2.534E-05	0.002708
11	$R_\rho = 2$, G = .015, H = 576, θ = .0001875	2.26E-01 1.631E-05	2.03E-01 4.151E-05	0.003401
12	$R_\rho = 2$, G = .015, H = 576, θ = .00025	2.84E-01 2.368E-05	2.69E-01 5.878E-05	0.002817
13	$R_\rho = 2$, G = .015, H = 576, θ = .0003125	2.54E-01 2.659E-05	2.40E-01 5.506E-05	0.002612
14	$R_\rho = 2$, G = .015, H = 576, θ = .000375	1.82E-01 2.202E-05	1.74E-01 5.180E-05	0.002321
15	$R_\rho = 2$, G = .015, H = 576, θ = .0004375	8.54E-02 1.323E-05	8.00E-02 3.048E-05	0.001849
16	$R_\rho = 2$, G = .015, H = 576, θ = .0005	4.70E-02 8.169E-06	4.49E-02 1.934E-05	0.001104
17	$R_\rho = 2$, G = .015, H = 576, θ = .0005625	7.33E-04 1.329E-06	7.16E-04 3.541E-06	0.0003492
18	$R_\rho = 2$, G = .015, H = 576, θ = .00625	3.55E-05 1.169E-06	3.51E-05 3.155E-06	-0.0006523
47	G = .015, H = 576, θ = .0025, $R_\rho = 1.2$	1.00E-01 1.899E-05	8.51E-02 2.72E-05	0.005156
48	G = .015, H = 576, θ = .0025, $R_\rho = 1.3$	1.14E-01 1.127E-05	9.59E-02 1.837E-05	0.004673
49	G = .015, H = 576, θ = .0025, $R_\rho = 1.4$	1.46E-01 1.422E-05	1.25E-01 2.421E-05	0.004585
62	G = .015, H = 576, θ = .0025, $R_\rho = 1.5$	1.34E-01 1.110E-05	1.15E-01 2.106E-05	0.004196
50	G = .015, H = 576, θ = .0025, $R_\rho = 1.6$	1.04E-01 8.459E-06	8.77E-02 1.706E-05	0.004109
69	G = .015, H = 576, θ = .0025, $R_\rho = 1.7$	1.19E-01 9.853E-06	1.03E-01 2.095E-05	0.004065
51	G = .015, H = 576, θ = .0025, $R_\rho = 1.8$	1.31E-01 1.019E-05	1.15E-01 2.263E-05	0.00401
52	G = .015, H = 576, θ = .0025, $R_\rho = 1.9$	1.50E-01 1.135E-05	1.31E-01 2.595E-05	0.004027

53	G = .015, H = 576, θ = .0025, R_ρ = 2.0	2.84E-01 2.368E-05	2.69E-01 5.878E-05	0.003328
54	G = .015, H = 576, θ = .0025, R_ρ = 2.1	1.39E-01 1.102E-05	1.22E-01 2.705E-05	0.003096
55	G = .015, H = 576, θ = .0025, R_ρ = 2.2	1.26E-01 1.007E-05	1.10E-01 2.578E-05	0.002758
56	G = .015, H = 576, θ = .0025, R_ρ = 2.3	1.08E-01 8.754E-06	9.49E-02 2.354E-05	0.002233
77	G = .015, H = 576, θ = .0025, R_ρ = 2.4	1.25E-01 9.61E-06	1.10E-01 2.684E-05	0.005156
57	G = .015, H = 576, θ = .0025, R_ρ = 2.5	8.60E-02 7.101E-06	7.53E-02 2.07E-05	0.002758
85	G = .015, H = 576, θ = .0025, R_ρ = 2.6	8.60E-02 6.92E-06	4.56E-02 2.103	0.004585
58	G = .015, H = 576, θ = .0025, R_ρ = 2.7	5.91E-02 5.161E-06	5.18E-02 1.636E-05	0.004196
59	R_ρ = 2, G = .015, H = 576, θ = .00375	9.95E-02 1.910E-05	9.48E-02 3.294E-05	0.003032
60	R_ρ = 2, G = .015, H = 576, θ = .004375	4.24E-02 1.164E-05	4.06E-02 2.03E-05	0.002146
61	R_ρ = 2, G = .015, H = 576, θ = .00375	1.74E-01 2.084E-05	1.56E-01 3.552E-05	0.002736
63	R_ρ = 2, G = .015, H = 576, θ = .0075	8.53136E-05 3.584E-05	8.18106E-05 7.159E-06	-0.008386
64	R_ρ = 2, G = .015, H = 576, θ = .006875	3.54E-03 4.138E-06	3.40E-03 8.068E-06	0.008449
65	R_ρ = 2, G = .015, H = 576, θ = .005	1.17E-01 1.801E-05	1.09E-01 3.084	0.003673
66	R_ρ = 2, G = .015, H = 576, θ = .00375	1.54E-01 1.672E-05	1.40E-01 3.248E-05	0.003898
67	R_ρ = 2, G = .015, H = 576, θ = .004375	1.01E-01 1.360E-05	9.28E-02 2.668E-05	0.003445
68	R_ρ = 2, G = .015, H = 576, θ = .005	5.85E-02 9.96E-06	5.47E-02 1.985E-05	0.002135
70	R_ρ = 2, G = .015, H = 576, θ = .005625	2.03E-02 5.590E-06	1.93E-02 1.161E-05	0.001757
71	R_ρ = 2, G = .015, H = 576, θ = .00625	9.78E-04 2.315E-06	9.40E-04 5.221E-06	0.0005237
72	R_ρ = 2, G = .015, H = 576, θ = .006875	5.14412E-05 2.171E-06	5.01312E-05 4.949E-06	-0.0009597
73	R_ρ = 2, G = .015, H = 576, θ = .0075	2.03111E-05 2.169E-06	1.96635E-05 4.947E-06	-0.002429
74	R_ρ = 2, G = .015, H = 576, θ = .000625	3.20E-02 2.108E-06	2.49E-02 7.474E-05	0.002335

75	R_ρ = 2, G = .015, H = 576, θ = .000125	7.27E-07 2.908E-06	5.88E-02 1.018E-05	0.002891
76	R_ρ = 2, G = .015, H = 576, θ = .0001875	1.38E-01 8.40E-06	1.18E-01 2.41E-05	0.00301
78	R_ρ = 2, G = .015, H = 576, θ = .0003125	7.44E-02 7.389E-06	6.68E-02 2.064E-05	0.00252
79	R_ρ = 2, G = .015, H = 576, θ = .000375	3.09E-02 4.306E-06	2.83E-02 1.230E-05	0.002039
80	R_ρ = 2, G = .015, H = 576, θ = .0004375	4.18E-03 1.41E-06	3.97E-03 4.32E-06	0.001316
81	R_ρ = 2, G = .015, H = 576, θ = .0005	3.22E-04 6.505E-07	3.17E-04 2.094E-06	0.0008244
82	R_ρ = 2, G = .015, H = 576, θ = .000625	3.29E-02 1.777E-06	2.59E-07 7.326E-06	0.002219
83	R_ρ = 2, G = .015, H = 576, θ = .000125	8.23E-02 5.63E-06	6.78E-02 1.937E-05	0.002651
84	R_ρ = 2, G = .015, H = 576, θ = .0001875	4.33E-02 7.971E-06	1.13E-01 2.452E-05	0.002449
86	R_ρ = 2, G = .015, H = 576, θ = .0003125	4.56E-02 4.902E-06	4.09E-02 7.697E-06	0.002269
87	R_ρ = 2, G = .015, H = 576, θ = .000375	1.50E-02 2.445E-06	1.3795E-02 1.495E-05	0.001777
88	R_ρ = 2, G = .015, H = 576, θ = .0004375	1.07E-03 6.941E-07	1.03E-03 2.371E-06	0.0007305
89	R_ρ = 2, G = .015, H = 576, θ = .0005	1.41E-04 4.459E-07	1.40E-04 1.563E-06	0.0002082
92	R_ρ = 2, θ = .0025, H = 576, G = .007	2.22E-03 1.172E-06	1.979E-03 3.129E-06	0.0006811
93	R_ρ = 2, θ = .0025, H = 576, G = .01	8.44E-02 5.486E-06	7.491E-02 1.302E-05	0.002359
94	R_ρ = 2, θ = .0025, H = 576, G = .025	1.23E-01 1.262E-05	1.12E-01 3.58E-05	0.005014
95	R_ρ = 2, θ = .0025, H = 576, G = .03	1.966E-01 1.643E-05	1.06E-01 4.494E-05	0.00521
96	R_ρ = 2, θ = .0025, H = 576, G = .05	1.335E-01 1.613E-05	1.20E-01 4.450E-05	0.005466
107	R_ρ = 2, G = .015, H = 100, θ = .000625	1.26E-01 1.007E-05.	1.10E-01 2.578E-05	0.0005305
108	R_ρ = 2, G = .015, H = 100, θ = .000125	2.08E-03 8.663E-06.	1.11E-03 2.374E-06	0.001457
109	R_ρ = 2, G = .015, H = 100, θ = .0001875	3.02E-03 8.339E-06	1.73E-03 2.243E-06	0.001965
110	R_ρ = 2, G = .015, H = 100, θ = .0025	5.49E-03 12.01E-05	3.74E-03 3.160E-06	0.002141

111	$R_\rho = 2$, G = .015, H = 100, θ = .0003125	7.87E-03 15.514E-05	5.71E-03 3.958E-06	0.002058
112	$R_\rho = 2$, G = .015, H = 100, θ = .000375	9.42E-03 19.927E-05	7.28E-03 4.767E-06	0.001898
113	$R_\rho = 2$, G = .015, H = 100, θ = .0004375	7.09E-03 17.703E-05	5.61E-03 4.398E-06	0.001384
114	$R_\rho = 2$, G = .015, H = 100, θ = .0005	1.36E-03 10.211E-05	1.02E-03 2.665E-06	0.0004797

LIST OF REFERENCES

Burnett, W., and J. Harding, 2002: Overview of operational ocean forecasting in the U.S. Navy: past, present & future. *Oceanography*, **15**, 4–12.

Figueroa, H. A., 1996: World ocean density ratios. *Journal of Physical Oceanography*, **26**, 267–275.

Ferrari, R., and G. Boccaletti, 2004: Eddy-mixed layer interactions in the ocean. *Oceanography*, **17**, 13–21.

Garrett, C., 1982: On the parameterization of diapycnal fluxes due to double-diffusive intrusions. *Journal of Physical Oceanography*, **12**, 952-959.

Garaud, P., 2010: Understanding the properties of fingering convection, with applications to oceanography and astrophysics. [Available at http://users.soe.ucsc.edu/~pgaraud/Research.html]

Jacobs, E., 2009: Current and planned Navy ocean modeling capability. http://www.ersl.noaa.gov/research/events/espc/9sep2010/jacobs_ocean)capability.pdf, accessed July, 2011.

Joyce, T. M., W. Zenk, and J. M. Toole, 1978: The anatomy of the Antarctic Polar Front in the Drake Passage. *Journal of Physical Research*, **83**, 6093–6113.

May, B. D., and D. E. Kelley, 2001: Growth and steady state stages of thermohaline intrusions in the Arctic Ocean. *Journal of Geophysical Research-Oceans*, **106,** 16783–16794.

Mei, C. C., and B. Vernescu, 2010: Homogenization methods for multiscale mechanics., *World Scientific Publishing*, 1–327.

Merryfield, W. J., G. Holloway, and A. E. Gargett, 1998: A global ocean model with double-diffusive mixing. *Journal of Physical Oceanography*, **29,** 1124–1142.

Peloquin, R., 1992: The Navy ocean modeling and prediction program. *Oceanography*, **5**, 4–8.

Radko, T., 2005: What determines the thickness of layers in a thermohaline staircase? *Journal of Fluid Mechanics*, **523**, 79–98.

——, 2007: Mechanics of merging events for a series of layers in a stratified turbulent fluid. *Journal of Fluid Mechanics*, **577,** 251–273.

Radko, T., and M. E. Stern, 1999: Salt fingers in three dimensions. *Journal of Marin Research*, **57,** 471–502.

Ruddick, B, n.d.: Thermohaline Intrusions. [Available online at http://www.phys.ocean.dal.ca/programs/doubdiff/demos/Thermohaline.html.]

Ruddick, B. and O. Kerr, 2003: Laboratory studies of interleaving. *Progress in Oceanography*, **56,** 529-547.

Ruddick, B., and O. Kerr, 2003a: Oceanic thermohaline intrusions: theory. *Progress in Oceanography*, **56,** 483–497.

——, 2003b: Oceanic thermohaline intrusions: theory. *Progress in Oceanography*, **56,** 483–497.

Ruddick, B., and A. E. Gargett, 2011: Oceanic double-diffusion: introduction. [Available at http://www.phys.ocean.dal.ca/programs/doubdiff/final_pdfs/Ruddick_Gargett_int.pdf.]

Ruddick, B., and K. Richards, 2003a: Oceanic thermohaline intrusions: observations. *Progress in Oceanography*, **56,** 499–527.

Ruddick, B. R., O. M. Phillips, and J. S. Turner, 1999: A laboratory and quantitative model of finite-amplitude thermohaline intrusions. *Dynamics of Atmospheres and Oceans*, **30,** 71–99.

Rudels, B. R., G. Bjork, R. D. Muench and U. Schauer, 1998: Double-diffusive layering in the Eurasian Basin of the Arctic Ocean. *Journal of Marine Systems*, **21**, 3–27.

Schmitt, R. W., J. R. Ledwell, E. T. Montgomery, K. L. Polzin, J. M. Toole, 2003: Enhanced diapycnal mixing by salt fingers in the thermocline of the tropical Atlantic. *Science Magazine*, **308**, 685–688.

Schmitt, R. W., 1979: The growth rate of supercritical salt fingers. *Deep-Sea Research*, **26A**, 23–44.

——, 1983: On density ratio balance in the central water. *Journal of Physical Oceanography*, **20**, 900–906.

Simeonov, J., and M. E. Stern, 2006: Equilibration of two-dimensional double-diffusive intrusions. *Journal of Physical Oceanography*, **37,** 625–643.

Stern, M. E., 1967: Lateral Mixing of Water Masses. *Deep-Sea Research*, **14,** 747–789.

Stern, M. E. and J. S. Turner, 1969: Salt fingers and convecting layers. *Deep-Sea Research*, **16**, 497-511.

Traxler, A., S. Stellmach, P. Garaud, T. Radko, and N. Brummell, 2010: Dynamics of fingering convection I: Small-scale fluxes and large scale instabilities. Submitted for consideration for publication in *Journal of Fluid Mechanics*.

Toole, J.M., and D. T. Georgi, 1981: In the dynamics and effects of double-diffusively driven intrusions. *Progress in Oceangraphy*, **10**, 123-145.

You, Y. (2002). A global ocean climatological atlas of the Turner angle: Implications for double-diffusion and water mass structure. *Deep-Sea Res.,* **49**, 2075–2093.

Zhang, J., 1998: Sensitivity of the GFDL modular ocean model to parameterization of double-diffusive processes. *Journal of Physical Oceanography*, **28**, 589–605.

THIS PAGE INTENTIONALLY LEFT BLANK

INITIAL DISTRIBUTION LIST

1. Defense Technical Information Center
   Ft. Belvoir, Virginia

2. Dudley Knox Library
   Naval Postgraduate School
   Monterey, California

3. Dr. Jeff Paduan
   Naval Postgraduate School
   Monterey, California

4. Dr. Timour Radko
   Naval Postgraduate School
   Monterey, California

5. Dr. Jason Flanagan
   Naval Postgraduate School
   Monterey, California